AVO analysis of P-, S-, and C-wave elastic and anelastic reflection data

Kris Innanen

ABSTRACT

Amplitudes vary in seismic reflection data in a complex manner. AVO problems (not to mention full waveform inversion and inverse scattering) must be supported by theory which: provides insight into the relationship between medium and amplitude, leads to modeling and inversion algorithms, and scales easily between rough-approximate and detailed-accurate tools for analysis. This applies equally to well-developed AVO regimes, such as P-, S-, and C-wave AVO, as it does to anelastic regimes. The purpose of this paper is to extend a mode of analysis elsewhere used to study anelastic inversion of P-P data, and to use it to discuss these regimes as well as anelastic AVF behaviour. A range of conclusions are arrived at: (1) second order corrections to converted wave amplitudes can account for dependence on target V_P, a dependence that is invisible to the Aki-Richards approximation. (2) Variations of anelastic reflection coefficients with angle and with frequency can be used to estimate target parameters such as Q_S. (3) To second order, a contrast in Q_S only across a boundary can cause a P-S mode conversion whereas a contrast in Q_P only cannot. (4) However, if a contrast occurs in both Q_P and Q_S but no other parameter, the Q_P contrast can alter the amplitude of the conversion. We also point out that in the nonlinear regime the Zoeppritz equations appear to be putting a premium on V_P/V_S ratios with a value of 2: expansion coefficients that couple density with all other parameters are of size $\propto (V_P/V_S - 2)$. In inversion, it is possible to express the recovery of Q_P and Q_S values in terms of the rate of change of the reflection coefficients with frequency.

INTRODUCTION

Amplitudes vary in seismic reflection data with tantalizing complexity. The full range of amplitude methods – from AVO analysis to full waveform inversion and inverse scattering – must be supported by theoretical descriptions that (1) provide the seismic explorationist with insight into the relationship between medium and amplitude, (2) lead directly to modeling and inversion algorithms, and (3) naturally allow the researcher to scale between rough-approximate (first order) and detailed-accurate (second order +) tools for analysis.

The benefit derivable from additional tools that fit this bill applies equally to AVO analysis in well-developed regimes, such as P-wave AVO, converted wave AVO and S-wave AVO, as to less fully developed model types, including anisotropic and anelastic regimes.

The purpose of this paper is to extend and more completely formalize a mode of analysis of seismic amplitudes used by Innanen (2011a) to study anelastic inversion of P-P data, and to use it to make a series of points of analysis regarding (1) elastic P-wave, S-wave, and converted wave AVO behaviour, and (2) the influence of anelasticity both on these three aspects of AVO, and on their (now non negligible) AVF behaviour as well.

In the elastic regime, seismic amplitude analysis typically carried out through use of the Aki-Richards (AR) and related approximations (Aki and Richards, 2002; Castagna and Backus, 1993). From it we may derive rough insight into, for instance, converted wave amplitudes. For instance, as pointed out by Stewart et al. (2002, 2003), target V_P is irrelevant to the converted wave amplitude within the AR approximation. However, this irrelevance does not persist for large contrasts and angles, and it would be beneficial to have a modeling framework capable of elucidating and quantify this fact—without losing the ease of analysis the AR approximation provides. It is to problems of this kind we apply ourselves in this paper.

In contrast to elastic problems, in the anelastic regime theory for amplitude behaviour has access to far fewer laboratory and/or field data with which to confirm or refute itself. Nevertheless, especially in recent years, theoretical studies (White, 1965; Chapman et al., 2006; Haase and Ursenbach, 2006; Lines et al., 2008; Quintal et al., 2009; Ren et al., 2009; Innanen, 2011a), laboratory studies (Lines et al., 2011a, and unpublished work of Sondergeld and Crowe), and field studies (Odebeatu et al., 2006; Bird and Innanen, 2011), working to identify and model anelastic reflectivity, have appeared in the literature in increasing number. Indeed in this very report all three types of contribution are discussed. In contrast to the elastic regime, almost everything about anelastic reflection strength approximations needs to be understood (the behaviour of *exact* solutions for viscoelastic boundaries has been more completely discussed by Borcherdt, 2009). Here we only begin to achieve this, but, we frame the problem and survey its properties.

The anelastic problem has required us to make some Q model choices which, while not arbitrary, do correspond to one or two of many possible models which best describe anelastic and dispersive reflection strengths. Indeed in this report Lines et al. (2011a) have generated lab results of an anelastic reflection which the models used in this paper would be hard-pressed to reproduced. What justifies our current choices is their ubiquity and simplicity; we choose the Q model reviewed by Aki and Richards (2002), which is a basic macroscopic Q model seen to (1) capture essential absorptive behaviour of seismic waves while (2) maintaining important physical properties such as linearity, causality, and a Q roughly independent of frequency.

In this paper we frame all our modeling in terms of plane waves and plane wave angles, as opposed to "true" AVO, for which a spherical wave, or point source-point receiver environment is required. Our justification for this is twofold: first, that the plane wave domain provides reasonable approximations within the angle range we consider in this paper, and second, that point source/point receiver AVO would begin with the plane wave analysis carried out here, and so can be considered a reasonable next step should the plane wave domain prove unsuitable.

Let us finally summarize the precise aspects of elastic and anelastic AVO that we next analyze and draw conclusions about. We determine that:

1. For elastic converted (PS) wave amplitudes:

   (a) Target V_P plays a small but nonnegligible (second order) role in determining in

$R_{\rm PS}$ amplitudes at small and moderate angles

2. For elastic SS wave amplitudes:
   (a) Target V_P plays a negligible (third order or higher) role in determining $R_{\rm SS}$ amplitudes for small and moderate angles
   (b) Target V_S plays a dominant role in second order corrections to the linear $R_{\rm SS}$ approximation
3. For anelastic PP amplitudes:
   (a) If target quality factors are low, the two anelastic perturbations (i.e., in Q_P and Q_S) included in addition to the standard V_P, V_S and ρ play a first order role in determining $R_{\rm PP}$
   (b) For large contrast targets, second order corrections to frequency-dependent anelastic AVO are required for accurate modeling
4. For anelastic converted (PS) wave amplitudes:
   (a) Target V_P/Q_P play little role in determining $R_{\rm PS}$ at 1st and 2nd order
   (b) $R_{\rm PS}$ exhibits non-negligible AVF behaviour given low target quality factors
   (c) Linear inversion formulas are available for anelastic $R_{\rm PS}$ AVF input data
   (d) A contrast in Q_S and only Q_S results in a P-S mode conversion
   (e) A contrast in Q_P and only Q_P causes a negligible P-S conversion, *but*
   (f) Given a simultaneous contrast in Q_P and Q_S and only Q_P and Q_S, the contrast in Q_P contributes non-negligibly to the strength of the P-S mode conversion
5. For anelastic shear (SS) wave amplitudes:
   (a) Target V_P and Q_P play negligible roles in determining $R_{\rm SS}$ amplitudes for small and moderate angles

The how and the why of an anelastic AVO/AVF workflow

Half of this paper concerns frequency-dependent AVO and amplitude-variation-with-frequency (AVF). It is one thing to analyze the mathematics of the Zoeppritz equations, having extended them to include anelasticity, and to claim that the resulting expressions are frequency dependent and should be studied that way. But how would one go about this?

AVF analysis, or AVO analysis in the presence of a strongly dispersive reflection, must be driven in practice by some suitable form of time-frequency decomposition of the traces. Let us schematically outline how this might be done (Bird and Innanen, 2011, have, for instance, used a fast S-transform). In Figure 1 we consider a conceptual representation of standard AVO analysis for later comparison. In Figure 1a, an NMO corrected reflection is plotted, with offset having been mapped to angle in some appropriate way. The event has

an evident AVO trend. Taking an amplitude profile along the peak, the AVO curve, which is roughly intepretable as $R(\theta)$, is then plotted in Figure 1b. This red curve is suitable for AVO analysis.

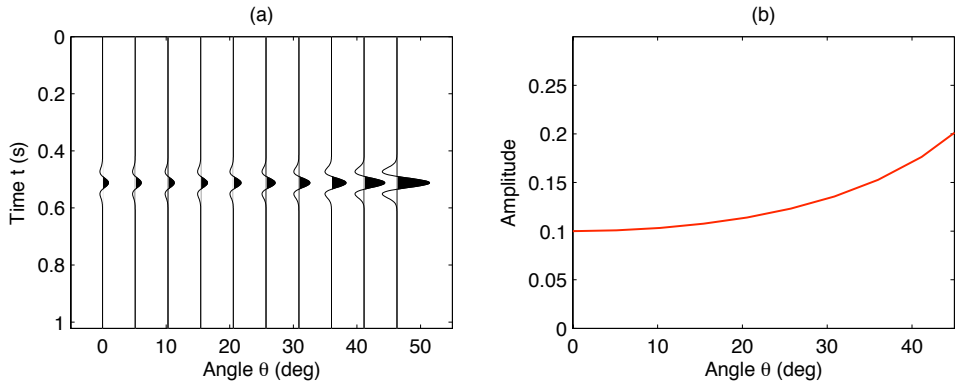

FIG. 1. Schematic illustrating AVO analysis. (a) An NMO-corrected event plotted against angle. (b) AVO curve extracted from (a).

Next, consider the case schematically depicted in Figure 2. In Figure 2a, an NMO-corrected panel containing three reflections is displayed. The middle one is suspected to correspond to a strong anelastic reflector, and therefore may carry within it the dispersive AVF signature of interest to us. We replace the wiggle plot for convenience now by an image plot (of the same data) in Figure 2b. Next, we apply some appropriate time-frequency decomposition to the data (e.g., Gabor transform or S-transform), forming a data cube (with variables θ, f, and t). We then pay special attention one time slice through this cube, the local spectrum of the event of interest, which lies between the two green lines. For fixed $t = 0.5s$, we then have a matrix of reflection amplitudes, whose real part is illustrated in Figure 2c. This matrix contains the reflection strengths as a function of angle and frequency.

In the presence of anelastic targets, where reflection strengths have a characteristic frequency (AVF) signature, in principle a different AVO curve is produced for any given frequency. We would appear to have two options for studying such amplitudes. We could (1) continue somewhat akin to the AVO analysis in Figure 1, by choosing a particular frequency as a parameter, then taking a profile similar to the red line in Figure 2d, extracting the AVO curve as in Figure 2e, and analyzing it, armed with some quantitative expectation of how the chosen f must alter the curve. Or, (2), we could by examine directly the AVF behaviour of the reflection, by choosing a fixed angle instead, and taking a profile similar to the blue line in Figure 2d. Extracting the AVF curve illustrated in Figure 2f, we might then analyze it in the context of appropriate anelastic theory.

In the next sections we provide some of the theory necessary for analysis of curves like those in Figures 2e-f to proceed. Before we do this, however, let us first provide some numerical evidence that this is a worthwhile exercise. In Figure 3 we plot $R_{\rm PP}$ and $R_{\rm PS}$ vs. incidence angle for a fixed, large contrast anelastic target, at several different frequencies. The black lines are the coefficients with infinite target Q_P, Q_S values. The blue and red lines are the anelastic AVO curves (both with target $Q_P = 30$ and $Q_S = 5$) at

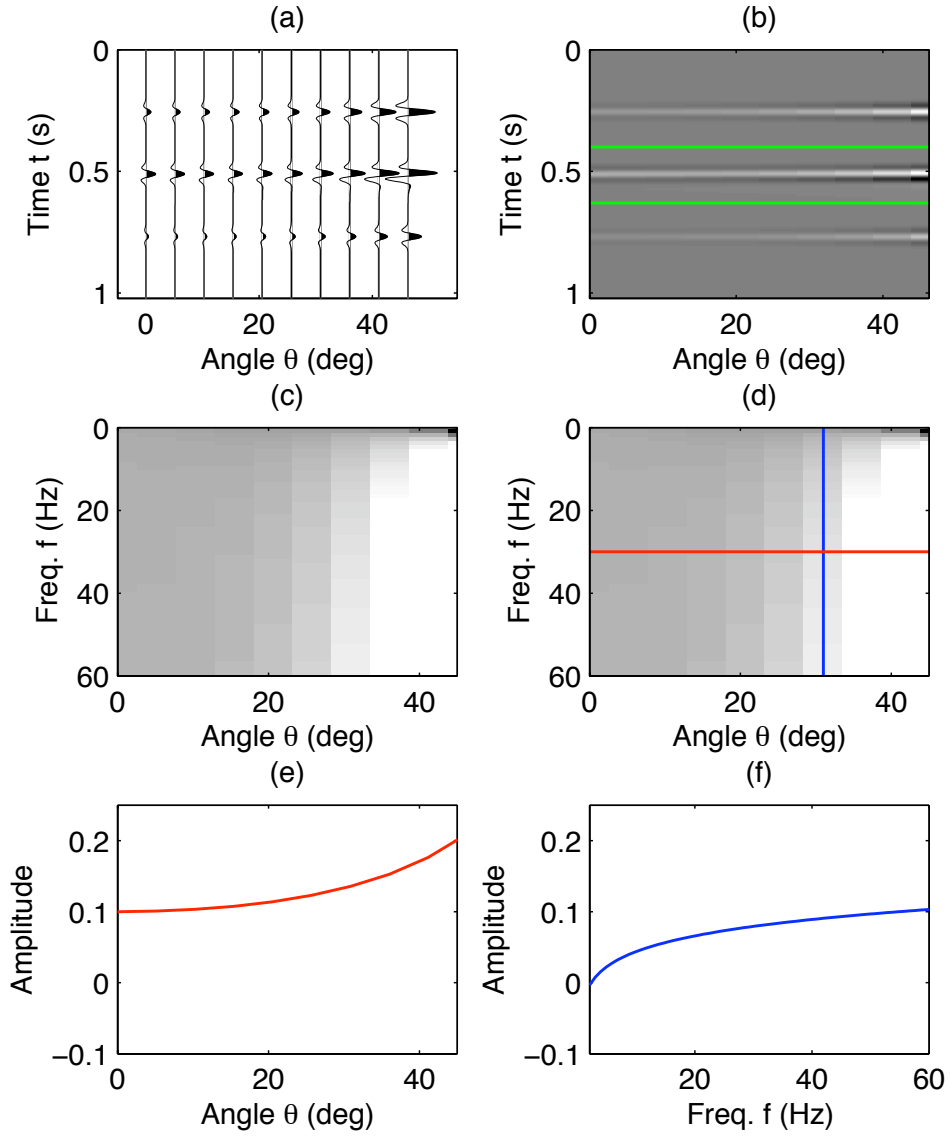

FIG. 2. Schematic of an AVO/AVF workflow. (a) An NMO-corrected gather with three events, the middle of which is suspected of being due to an anelastic contrast. (b) The same data plotted in image form. A sequence of time-frequency decompositions is carried out, which includes a time-local analysis of the data between the green lines. (c) The result is an amplitude matrix with independent variables frequency f and angle θ. (d) Frequency dependent AVO analysis is carried out by fixing f_0 and extracting the AVO curve (red); AVF analysis is carried out by fixing θ_0 and extracting an AVF curve (blue). (e)–(f) The extracted curves ready to drive analysis and/or inversion.

two representative frequencies.

In Figures 3a-b we compare the curves over the whole angle range. For both fixed frequencies (blue and red), the presence of anelasticity appears to "soften" the response, smoothing and dimming the variation at and around the critical angle seen in the elastic equivalent (black). In these critical and post critical domains the influence of anelasticity is evidently quite important.

However, most AVO processing and interpretation occurs well before critical angle. In Figures 3c-d we zoom in on the same curves at lower angles. Still, here, we detect possibly important differences in curve slope and/or intercept for anelastic targets, which vary depending on which representative frequency is analyzed. Beyond academic interest, there are, therefore, practical reasons to analyze the anelastic reflection problem, such that these variations are understood and accounted for in AVO analysis.

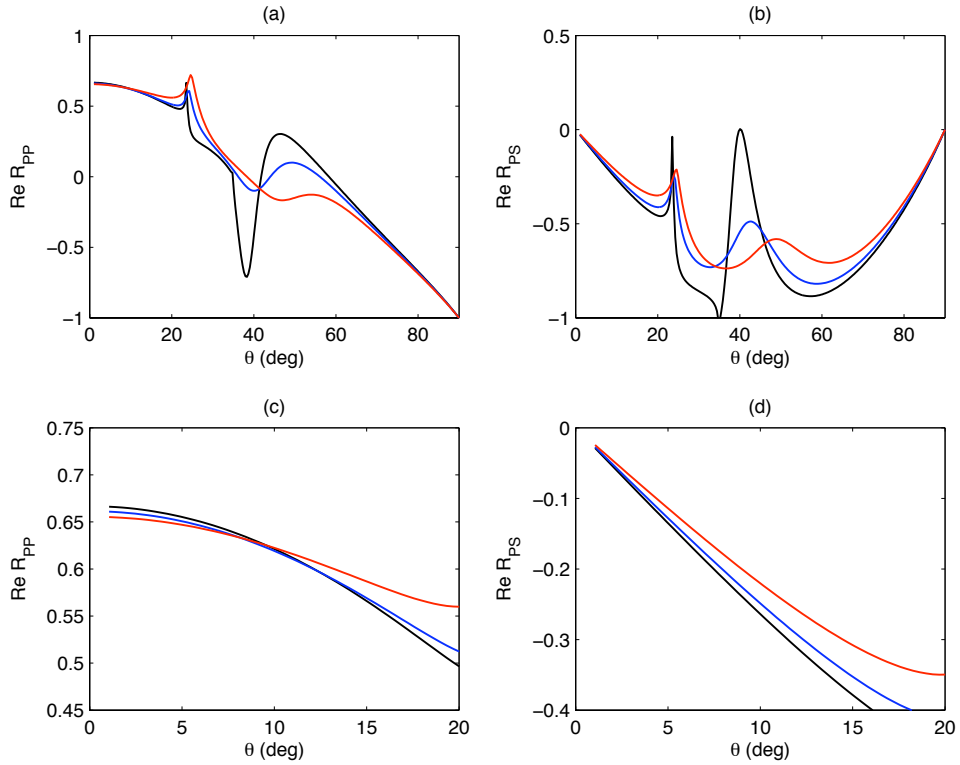

FIG. 3. AVO curves for R_{PP} and R_{PS} modeled above an anelastic target. Incidence medium parameters: $V_{P_0} = 2000$m/s, $V_{S_0} = 1500$m/s, $\rho_0 = 2.0$gm/cc, with infinite quality factors. Target medium parameters: $V_{P_1} = 5000$m/s, $V_{S_1} = 3500$m/s, $\rho_1 = 4.0$gm/cc, $Q_{P_1} = 30$, and $Q_{S_1} = 5$. Black line: R_{PP} and R_{PS} with target

THEORY AND FORMULATION

In this section we formulate exact, linearized and approximate nonlinear AVO by expanding certain convenient matrix forms of the Knott-Zoeppritz equations. We then discuss direct inversion of these relationships to form target elastic parameter estimation algorithms.

I. Basic equations and solutions

We begin with matrix forms of the Knott-Zoeppritz equations (which are framed in a convenient way in this report by Innanen, 2011b). Letting θ_0 and ϕ_0 represent the incident P- and S-wave angles respectively, and parametrizing in terms of $X = \sin\theta_0$, $Y = \sin\phi_0$,

we have

$$\mathbf{P}\begin{bmatrix} R_{\rm PP} \\ R_{\rm PS} \\ T_{\rm PP} \\ T_{\rm PS} \end{bmatrix} = \mathbf{b}_P, \quad \text{and} \quad \mathbf{S}\begin{bmatrix} R_{\rm SS} \\ R_{\rm SP} \\ T_{\rm SS} \\ T_{\rm SP} \end{bmatrix} = \mathbf{b}_S, \tag{1}$$

where

$$\mathbf{P} \equiv \begin{bmatrix} -X & -\Gamma_B(X) & CX & \Gamma_D(X) \\ \Gamma_1(X) & -BX & \Gamma_C(X) & -DX \\ 2B^2X\Gamma_1(X) & B\Gamma^B(X) & 2AD^2X\Gamma_C(X) & AD\Gamma^D(X) \\ -\Gamma^B(X) & 2B^2X\Gamma_B(X) & 2AC\Gamma^D(X) & -2AD^2X\Gamma_D(X) \end{bmatrix}, \tag{2}$$

$$\mathbf{S} \equiv \begin{bmatrix} -\Gamma_1(Y) & -B'Y & \Gamma_F(Y) & EY \\ Y & -\Gamma_{B'}(Y) & FY & -\Gamma_E(Y) \\ \Gamma^1(Y) & 2Y\Gamma_{B'}(Y) & AF\Gamma^F(Y) & 2AF^2Y\Gamma_E(Y) \\ -2Y\Gamma_1(Y) & B'\Gamma^1(Y) & 2AF^2Y\Gamma_F(Y) & -AE\Gamma^F(Y) \end{bmatrix}, \tag{3}$$

and

$$\mathbf{b}_P \equiv \begin{bmatrix} X \\ \Gamma_1(X) \\ 2B^2X\Gamma_1(X) \\ \Gamma^B(X) \end{bmatrix}, \quad \text{and} \quad \mathbf{b}_S \equiv \begin{bmatrix} \Gamma_1(Y) \\ Y \\ \Gamma_1(Y) \\ 2Y\Gamma_1(Y) \end{bmatrix}, \tag{4}$$

and using ratios

$$A \equiv \frac{\rho_1}{\rho_0}, \quad B \equiv \frac{V_{S_0}}{V_{P_0}}, \quad B' \equiv \frac{V_{P_0}}{V_{S_0}}, \quad C \equiv \frac{V_{P_1}}{V_{P_0}}, \quad D \equiv \frac{V_{S_1}}{V_{P_0}}, \quad E \equiv \frac{V_{P_1}}{V_{S_0}}, \quad F \equiv \frac{V_{S_1}}{V_{S_0}}, \tag{5}$$

and the functions

$$\begin{aligned} \Gamma_j(Z) &\equiv \sqrt{1 - j^2Z^2}, \\ \Gamma^j(Z) &\equiv 1 - 2j^2Z^2. \end{aligned} \tag{6}$$

Any one of the four displacement reflection coefficients can be determined from the above equations using Cramer's rule. Forming two auxiliary matrices $\mathbf{P}_P$ and $\mathbf{P}_S$ by replacing the first and then second columns of $\mathbf{P}$ with $\mathbf{b}_P$, and then forming a further two auxiliary matrices $\mathbf{S}_S$ and $\mathbf{S}_P$ by replacing the first and then second columns of $\mathbf{S}$ with $\mathbf{b}_S$, we have

$$R_{\rm PP} = \frac{\det\mathbf{P}_P}{\det\mathbf{P}}, \quad R_{\rm PS} = \frac{\det\mathbf{P}_S}{\det\mathbf{P}}, \quad R_{\rm SS} = \frac{\det\mathbf{S}_S}{\det\mathbf{S}}, \quad R_{\rm SP} = \frac{\det\mathbf{S}_P}{\det\mathbf{S}}. \tag{7}$$

II. Series expansion and approximation

The aim is to understand the response of the reflection coefficients to contrasts in the elastic (or anelastic) parameters across a target boundary. Let us adjust the equations above so that they more directly help with this. We begin by re-expressing certain of the elastic

parameter ratios A–F in equation (5) in terms of perturbations that measure these contrasts. We define

$$a_{VP} \equiv 1 - \frac{V_{P_0}^2}{V_{P_1}^2}, \quad a_{VS} \equiv 1 - \frac{V_{S_0}^2}{V_{S_1}^2}, \quad a_\rho \equiv 1 - \frac{\rho_0}{\rho_1}, \tag{8}$$

in which case

$$\begin{aligned} A &= (1-a_\rho)^{-1} = 1 + a_\rho + a_\rho^2 + a_\rho^3 + ... \\ C &= (1-a_{VP})^{-1/2} = 1 + \frac{1}{2}a_{VP} + \frac{3}{8}a_{VP}^2 + \frac{5}{16}a_{VP}^3 + ... \\ F &= (1-a_{VS})^{-1/2} = 1 + \frac{1}{2}a_{VS} + \frac{3}{8}a_{VS}^2 + \frac{5}{16}a_{VS}^3 + ..., \end{aligned} \tag{9}$$

and consequently

$$\begin{aligned} D = BF &= B\left(1 + \frac{1}{2}a_{VS} + \frac{3}{8}a_{VS}^2 + \frac{5}{16}a_{VS}^3 + ...\right), \\ E = B'C &= B'\left(1 + \frac{1}{2}a_{VP} + \frac{3}{8}a_{VP}^2 + \frac{5}{16}a_{VP}^3 + ...\right). \end{aligned} \tag{10}$$

Because B and B' are ratios of incidence medium parameters, and thus contain no target medium information, we do not expand them. The elements of $\mathbf{P}_P$, $\mathbf{P}_S$, $\mathbf{S}_S$, and $\mathbf{S}_P$, having had these expressions substituted into them, are close now to expressing themselves directly in orders of the perturbations a_{VP}, a_{VS}, and a_ρ. The remaining wrinkle is that these perturbations occasionally occur within $\Gamma_j(Z)$ type functions, i.e., under a radical sign. But by making use of a final expansion

$$\Gamma_j(Z) = (1 - j^2Z^2)^{1/2} = 1 - \frac{1}{2}(jZ)^2 - \frac{1}{8}(jZ)^4 - ..., \tag{11}$$

each element of $\mathbf{P}_P$, $\mathbf{P}_S$, $\mathbf{S}_S$, and $\mathbf{S}_P$ now appear directly as series in powers of the three perturbations. The next problem is to express the reflection coefficients (which, according to equation (7), are ratios of determinants of the matrices) this way too.

The determinant of a matrix is a linear combination of products of elements of the matrix. Hence, if the elements of the matrix are series in orders of the perturbations, so must be the determinants. Let us organize them into terms that are zeroth, first, second, etc. order in any of a_{VP}, a_{VS}, and a_ρ:

$$\begin{aligned} \det\mathbf{P}_P &= \det\mathbf{P}_{P_1} + \det\mathbf{P}_{P_2} + \det\mathbf{P}_{P_3} + ..., \\ \det\mathbf{P}_S &= \det\mathbf{P}_{S_1} + \det\mathbf{P}_{S_2} + \det\mathbf{P}_{S_3} + ..., \\ \det\mathbf{P} &= \det\mathbf{P}_0 + \det\mathbf{P}_1 + \det\mathbf{P}_2 + \det\mathbf{P}_3 + ..., \end{aligned} \tag{12}$$

and

$$\begin{aligned} \det\mathbf{S}_P &= \det\mathbf{S}_{P_1} + \det\mathbf{S}_{P_2} + \det\mathbf{S}_{P_3} + ..., \\ \det\mathbf{S}_S &= \det\mathbf{S}_{S_1} + \det\mathbf{S}_{S_2} + \det\mathbf{S}_{S_3} + ..., \\ \det\mathbf{S} &= \det\mathbf{S}_0 + \det\mathbf{S}_1 + \det\mathbf{S}_2 + \det\mathbf{S}_3 + ..., \end{aligned} \tag{13}$$

where the subscript refers to order in any combination of the perturbations*. In carrying out this organization, one notices that only det$\mathbf{P}$ and det$\mathbf{S}$ have zeroth order terms; none of the auxiliary matrices do. This reflects the fact that reflections require contrasts: if any of det$\mathbf{P}_P$, det$\mathbf{P}_S$, det$\mathbf{S}_S$, or det$\mathbf{S}_P$ had terms that were zeroth order in a_{VP}, a_{VS}, and a_ρ, by inspection of equation (7) it is clear that nonzero reflection coefficients would be predicted even when no contrasts were present. Dividing through by these zeroth order terms we may instead write

$$\begin{aligned}
\hat{\det}\mathbf{P}_P &= \hat{\det}\mathbf{P}_{P_1} + \hat{\det}\mathbf{P}_{P_2} + \hat{\det}\mathbf{P}_{P_3} + ..., \\
\hat{\det}\mathbf{P}_S &= \hat{\det}\mathbf{P}_{S_1} + \hat{\det}\mathbf{P}_{S_2} + \hat{\det}\mathbf{P}_{S_3} + ..., \\
\hat{\det}\mathbf{P} &= 1 + \hat{\det}\mathbf{P}_1 + \hat{\det}\mathbf{P}_2 + \hat{\det}\mathbf{P}_3 + ...,
\end{aligned} \tag{14}$$

and

$$\begin{aligned}
\hat{\det}\mathbf{S}_P &= \hat{\det}\mathbf{S}_{P_1} + \hat{\det}\mathbf{S}_{P_2} + \hat{\det}\mathbf{S}_{P_3} + ..., \\
\hat{\det}\mathbf{S}_S &= \hat{\det}\mathbf{S}_{S_1} + \hat{\det}\mathbf{S}_{S_2} + \hat{\det}\mathbf{S}_{S_3} + ..., \\
\hat{\det}\mathbf{S} &= 1 + \hat{\det}\mathbf{S}_1 + \hat{\det}\mathbf{S}_2 + \hat{\det}\mathbf{S}_3 + ...,
\end{aligned} \tag{15}$$

where the hat signifies division by the zeroth order term det$\mathbf{P}_0$ or det$\mathbf{S}_0$ as the case may be. Since the reflection coefficients are ratios of these determinants, such division will have no effect on the final result. Finally, now since $\hat{\det}\mathbf{P}_1 + \hat{\det}\mathbf{P}_2 + \hat{\det}\mathbf{P}_3 + ...$ and $\hat{\det}\mathbf{S}_1 + \hat{\det}\mathbf{S}_2 + \hat{\det}\mathbf{S}_3 + ...$ are at least first order in a_{VP}, a_{VS}, and a_ρ, for small contrasts and small angles we may reasonably assume them to be less than unity. So, we may expand the reflection coefficients as

$$\begin{aligned}
R_{\text{PP}} &= \frac{\hat{\det}\mathbf{P}_P}{1 + \hat{\det}\mathbf{P}_1 + \hat{\det}\mathbf{P}_2 + ...} = \hat{\det}\mathbf{P}_{P_1} + \left(\hat{\det}\mathbf{P}_{P_2} + \hat{\det}\mathbf{P}_{P_1}\hat{\det}\mathbf{P}_1\right) + ..., \\
R_{\text{PS}} &= \frac{\hat{\det}\mathbf{P}_S}{1 + \hat{\det}\mathbf{P}_1 + \hat{\det}\mathbf{P}_2 + ...} = \hat{\det}\mathbf{P}_{S_1} + \left(\hat{\det}\mathbf{P}_{S_2} + \hat{\det}\mathbf{P}_{S_1}\hat{\det}\mathbf{P}_1\right) + ..., \\
R_{\text{SS}} &= \frac{\hat{\det}\mathbf{S}_S}{1 + \hat{\det}\mathbf{S}_1 + \hat{\det}\mathbf{S}_2 + ...} = \hat{\det}\mathbf{S}_{S_1} + \left(\hat{\det}\mathbf{S}_{S_2} + \hat{\det}\mathbf{S}_{S_1}\hat{\det}\mathbf{S}_1\right) + ..., \\
R_{\text{SP}} &= \frac{\hat{\det}\mathbf{S}_P}{1 + \hat{\det}\mathbf{S}_1 + \hat{\det}\mathbf{S}_2 + ...} = \hat{\det}\mathbf{S}_{P_1} + \left(\hat{\det}\mathbf{S}_{P_2} + \hat{\det}\mathbf{S}_{P_1}\hat{\det}\mathbf{S}_1\right) + ...,
\end{aligned} \tag{16}$$

up to any desired order.

III. Inversion and target estimation formulas

Up to this point we have been as general as possible in our development. We are also concerned with the inversion of these relationships, wherein measurements of R_{PP}, R_{PS}, R_{SS} and R_{SP} are used to estimate the perturbations a_{VP}, a_{VS}, and a_ρ that define the reflecting boundary. But, it appears to be less instructive to discuss inverting equation

*Meaning, for instance, that a_ρ^3 and $a_{V_P}a_{V_S}^2$ are both third order, and so forth.

(16) with the same level of generality that was used in deriving it, and more instructive to illustrate it for a particular case. Let us do that here, but in keeping with the rest of this section nevertheless focus on its general character.

Taking a set of incidence and target medium parameters and following the prescription in equations (1)–(16) we may generate approximations of any of the four elastic displacement reflection coefficients R_{PP}, R_{PS}, R_{SS} and R_{SP} up to (in principle) any level of accuracy assuming convergence of the various series. What that means in practice, to take R_{PP} as an example, is that we determine the coefficients Δ in the series

$$R_{\text{PP}}(\theta_0) = R^{(1)}_{\text{PP}}(\theta_0) + R^{(2)}_{\text{PP}}(\theta_0) + ..., \tag{17}$$

where

$$R^{(1)}_{\text{PP}}(\theta_0) = \Delta_p(\theta_0)a_{VP} + \Delta_s(\theta_0)a_{VS} + \Delta_\rho(\theta_0)a_\rho, \tag{18}$$

and

$$\begin{aligned} R^{(2)}_{\text{PP}}(\theta_0) =& \Delta_{pp}(\theta_0)a^2_{VP} + \Delta_{ps}(\theta_0)a_{VP}a_{VS} + \Delta_{p\rho}(\theta_0)a_{VP}a_\rho \\ &+ \Delta_{ss}(\theta_0)a^2_{VS} + \Delta_{s\rho}(\theta_0)a_{VS}a_\rho + \Delta_{\rho\rho}(\theta_0)a^2_\rho, \end{aligned} \tag{19}$$

etc., as being

$$\begin{aligned} &\Delta_p(\theta_0) = \frac{1}{4}\left(1 + \sin^2\theta_0\right), && \Delta_s(\theta_0) = -2B^2\sin^2\theta_0, \\ &\Delta_\rho(\theta_0) = \frac{1}{2}\left(1 - 4B^2\sin^2\theta_0\right), && \Delta_{pp}(\theta_0) = \frac{1}{8} + \frac{1}{4}\sin^2\theta_0, \\ &\Delta_{ps}(\theta_0) = 0, \quad \Delta_{p\rho}(\theta_0) = 0, && \Delta_{ss}(\theta_0) = B^2(B-2)\sin^2\theta_0, \\ &\Delta_{s\rho}(\theta_0) = B^2(2B-1)\sin^2\theta_0, && \Delta_{\rho\rho}(\theta_0) = \frac{1}{4} - B\left(\frac{1}{4} + B - B^2\right)\sin^2\theta_0, \end{aligned} \tag{20}$$

having truncated the series in equation (11) beyond first order in $\sin^2\theta_0$. With expressions like (17) in hand[†] we may derive formulas for the recovery of a_{VP}, a_{VS}, and a_ρ directly from measurements of the reflection coefficients. The approach is to expand the perturbations themselves in series,

$$\begin{aligned} a_{VP} &= a_{VP_1} + a_{VP_2} + a_{VP_3} + ..., \\ a_{VS} &= a_{VS_1} + a_{VS_2} + a_{VS_3} + ..., \\ a_\rho &= a_{\rho_1} + a_{\rho_2} + a_{\rho_3} + ..., \end{aligned} \tag{21}$$

where for instance a_{VP_n} is that component of a_{VP} that is nth order in $R_{\text{PP}}(\theta_0)$. These series are substituted into equation (17)—and/or any others like it—and like orders are equated,

[†]To actually move through equations (1)–(16) to determine the coefficients in equation (20), I used the symbolic math tools in Maple. Mathematica would no doubt be just as good, and probably a lot prettier. It is a perfect problem for a symbolic math program: nothing very complicated, but many multiplications of multinomials, many instances of re-organization of the results, and many truncations of series at chosen orders of many variables.

following the argumentation applied in the more complete elastic wave theories of inverse scattering (e.g., Weglein et al., 2003; Zhang and Weglein, 2009). At first order, we have

$$R_{\text{PP}}(\theta_0) = \Delta_p(\theta_0)a_{VP_1} + \Delta_s(\theta_0)a_{VS_1} + \Delta_\rho(\theta_0)a_{\rho_1}, \tag{22}$$

at second order,

$$\mathcal{R}^{(2)}_{PP}(\theta_0) = \Delta_p(\theta_0)a_{VP_2} + \Delta_s(\theta_0)a_{VS_2} + \Delta_\rho(\theta_0)a_{\rho_2}, \tag{23}$$

where

$$\begin{aligned}\mathcal{R}^{(2)}_{PP}(\theta_0) \equiv &\Delta_{pp}(\theta_0)a^2_{VP_1} + \Delta_{ps}(\theta_0)a_{VP_1}a_{VS_1} + \Delta_{p\rho}(\theta_0)a_{VP_1}a_{\rho_1} \\ &+ \Delta_{ss}(\theta_0)a^2_{VS_1} + \Delta_{s\rho}(\theta_0)a_{VS_1}a_{\rho_1} + \Delta_{\rho\rho}(\theta_0)a^2_{\rho_1},\end{aligned} \tag{24}$$

and so on. Given a set of angles $\Theta_0 = \{\theta_0^{(1)}, \theta_0^{(2)}, \theta_0^{(3)}, ..., \theta_0^{(N)}\}$, with $N \geq 3$, at which data R_{PP} are available, such that equation (22) becomes a system of N equations

$$\begin{bmatrix} R_{\text{PP}}(\theta_0^{(1)}) \\ R_{\text{PP}}(\theta_0^{(2)}) \\ \vdots \\ R_{\text{PP}}(\theta_0^{(N)}) \end{bmatrix} = \mathbf{D} \begin{bmatrix} a_{VP_1} \\ a_{VS_1} \\ a_{\rho_1} \end{bmatrix} \tag{25}$$

where

$$\mathbf{D} = \begin{bmatrix} \Delta_p(\theta_0^{(1)}) & \Delta_s(\theta_0^{(1)}) & \Delta_\rho(\theta_0^{(1)}) \\ \Delta_p(\theta_0^{(2)}) & \Delta_s(\theta_0^{(2)}) & \Delta_\rho(\theta_0^{(2)}) \\ \vdots & \vdots & \vdots \\ \Delta_p(\theta_0^{(N)}) & \Delta_s(\theta_0^{(N)}) & \Delta_\rho(\theta_0^{(N)}) \end{bmatrix}, \tag{26}$$

we may solve the (likely overdetermined) system for $[a_{VP_1}, a_{VS_1}, a_{\rho_1}]^T$ in e.g., the least-squares sense through

$$\begin{bmatrix} a_{VP_1}(\Theta_0) \\ a_{VS_1}(\Theta_0) \\ a_{\rho_1}(\Theta_0) \end{bmatrix} = \left(\mathbf{D}^T\mathbf{D}\right)^{-1}\mathbf{D}^T \begin{bmatrix} R_{\text{PP}}(\theta_0^{(1)}) \\ R_{\text{PP}}(\theta_0^{(2)}) \\ \vdots \\ R_{\text{PP}}(\theta_0^{(N)}) \end{bmatrix}; \tag{27}$$

by adding the argument Θ_0 to the three linear perturbations we emphasize that these reconstructions do depend on the choice of input angles. When determined, the three quantities in equation (27) may be interpreted as approximate reconstructions of the perturbations. Or, if the contrasts are too large for a linear approximation to be valid, the same three quantities may be combined using equation (24) to generate the second order data-like quantity $\mathcal{R}^{(2)}_{PP}$. Then, because of the close relationship born between equations (22) and (23), the second order terms a_{VP_2}, a_{VS_2}, and a_{ρ_2} may be solved for using the same least squares formulation, but using $\mathcal{R}^{(2)}_{PP}(\Theta_0)$ instead of $R_{\text{PP}}(\Theta_0)$. This inverse procedure may continue to any desired order.

AVO AND ELASTIC TARGETS

Innanen (2011a) has used the above framework to model and invert the AVO and AVF signatures of anelastic P-P reflections. In the next section we will reconsider the anelastic problem and extend it. Here we will remain in the elastic regime, but focus on converted wave and S-wave amplitude modeling and inversion.

Elastic converted wave AVO and the influence of V_P contrasts

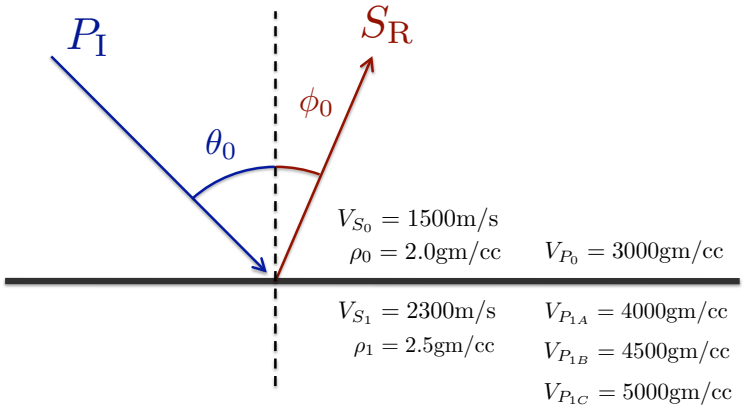

FIG. 4. A test elastic model for comparison of R_{PS} curves and the influence of target V_P thereon. All incidence medium properties are fixed as shown. Target density and S-wave velocity are fixed also. Three target V_P values are chosen as shown.

A major reason for posing the forward and inverse AVO problems as we have is that it makes analysis straightforward, even in regimes that are otherwise the purview of numerics and guesswork, namely, where nonlinearity and large contrasts arise. As an example, let us consider the influence of the target P-wave velocity on R_{PS}.

We carry out the expansion for R_{PS} in equation (16). Linearly in a_{VP}, a_{VS}, and a_ρ, we obtain

$$R_{\mathrm{PS}}(\theta_0) \approx \Lambda_p(\theta_0)a_{VP} + \Lambda_s(\theta_0)a_{VS} + \Lambda_\rho(\theta_0)a_\rho, \tag{28}$$

where

$$\Lambda_p(\theta_0) = 0, \quad \Lambda_s(\theta_0) = -B\sin\theta_0, \quad \text{and} \quad \Lambda_\rho(\theta_0) = -\left(B + \frac{1}{2}\right)\sin\theta_0. \tag{29}$$

Although it is different in its detail, this approximation is in its bulk accuracy similar to the Aki-Richards approximation of R_{PS} (Aki and Richards, 2002), if in the latter we replace the average incidence/transmission angles with "plain" incidence angles. And like in that approximation (as is pointed out by, e.g., Stewart et al., 2002), the most striking feature of equation (28) is the nullity of $\Lambda_p(\theta_0)$. Evidently, R_{PS} is, to first order, unaffected by variations in P-wave velocity.

This only approximately true. In Figure 4 we establish a set of three test elastic models with varying target V_P values, but with all other properties, including V_S and ρ unchanged

in the incidence and target mediums. To the extent that equation (28) is accurate, these models should all produce the same $R_{\rm PS}$ curves.

The exact curves are plotted in Figure 5a–c. It is clear that changes to the target P-wave velocity certainly do affect the $R_{\rm PS}$ behaviour, though to be sure we also see why the linear approximation neglects its influence, since the three curves are very close to one another at small angle.

In Figure 5d–f we compare the exact $R_{\rm PS}$ curves (black) with the linearizations of equation (28) (red). All three red curves are, of course, the same. Well short of the critical angle these approximations appear to capture the basic trend of all three exact curves, but a close examination (Figure 5g–i) reveals that errors in magnitude and slope are present in all cases, and these depend in their detail on the P-wave velocity contrast.

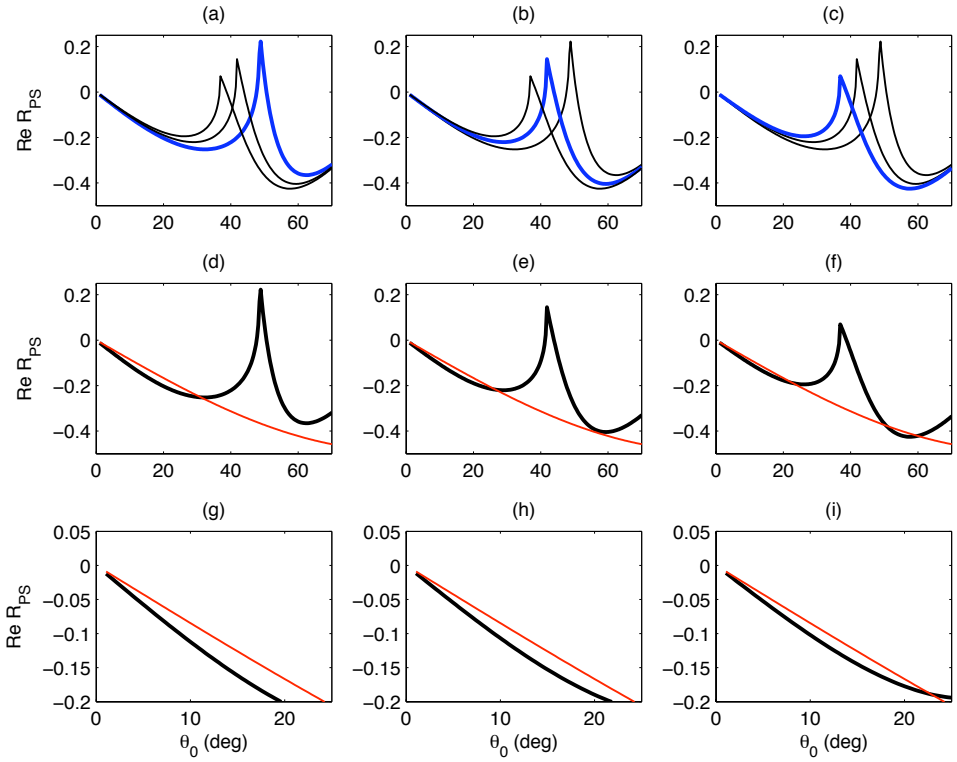

FIG. 5. Exact and approximate $R_{\rm PS}$ curves corresponding to the models in Figure 4: (a)–(c) blue curves correspond to exact $R_{\rm PS}$ over V_{P_1A}, V_{P_1B} and V_{P_1C} respectively; (d)–(f) black curves are the exact $R_{\rm PS}$, and the red curves correspond to the linear approximate forms in equation (28); (g)–(i) zoom in on (d)–(f) at small angles.

We may give these numerical observations some analytic context by including no more than one further order to the $R_{\rm PS}$ approximation. Continuing to follow the prescription from the previous section, we obtain

$$R_{\rm PS}(\theta_0) = R^{(1)}_{\rm PS}(\theta_0) + R^{(2)}_{\rm PS}(\theta_0) + ..., \tag{30}$$

where

$$R^{(1)}_{\rm PS}(\theta_0) = \Lambda_p(\theta_0)a_{VP} + \Lambda_s(\theta_0)a_{VS} + \Lambda_\rho(\theta_0)a_\rho, \tag{31}$$

and

$$R^{(2)}_{\rm PS}(\theta_0) = \Lambda_{pp}(\theta_0)a^2_{VP} + \Lambda_{ps}(\theta_0)a_{VP}a_{VS} + \Lambda_{p\rho}(\theta_0)a_{VP}a_\rho + \Lambda_{ss}(\theta_0)a^2_{VS} + \Lambda_{s\rho}(\theta_0)a_{VS}a_\rho + \Lambda_{\rho\rho}(\theta_0)a^2_\rho, \tag{32}$$

etc., and

$$\begin{aligned} &\Lambda_p(\theta_0) = 0, \quad \Lambda_s(\theta_0) = -B\sin\theta_0, \quad \Lambda_\rho(\theta_0) = -\left(B + \frac{1}{2}\right)\sin\theta_0, \\ &\Lambda_{pp}(\theta_0) = 0, \quad \Lambda_{ps}(\theta_0) = \frac{1}{4}B\sin\theta_0, \quad \Lambda_{ss}(\theta_0) = -\frac{3}{4}B\sin\theta_0, \\ &\Lambda_{p\rho}(\theta_0) = \Lambda_{s\rho}(\theta_0) = \frac{1}{4}\left(B - \frac{1}{2}\right)\sin\theta_0, \quad \Lambda_{\rho\rho}(\theta_0) = -\frac{1}{2}\sin\theta_0. \end{aligned} \tag{33}$$

The non-dominant role which target V_P plays is still visible at second order, where we see that the a^2_{VP} term remains nil. Its influence is enacted through coupling with the density and S-wave velocity terms, as can be discerned from the nonzero factors $\Lambda_{ps}(\theta_0)$ and $\Lambda_{p\rho}(\theta_0)$. And indeed, by including these terms in the $R_{\rm PS}$ approximation, as we do in Figure 6, a significantly increased capture of the small angle behaviour of the coefficient is noted.

Finally, we can confirm that a portion of this corrective amplitude adjustment is due to these two terms by plotting the approximation with (red) and without them (blue), in Figure 7.

In summary, the series expansion allows us to—as necessary—add terms to generate numerically more accurate approximations of seismic amplitudes. Also, the relative importance of individual parameters can be predicted by their coefficients, which may be null at some orders but finite at others.

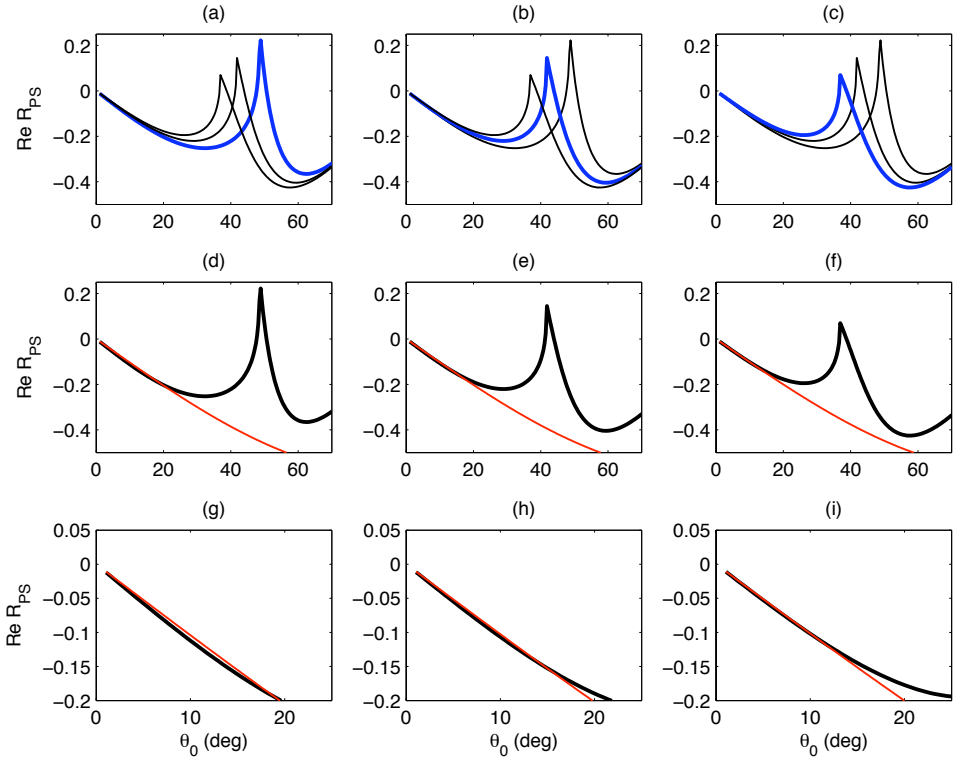

FIG. 6. Repeat of Figure 5, but with the second-order accurate $R_{\rm PS}$ approximation plotted in red in (d)–(i). The bottom row in comparison with the bottom row of Figure 5 illustrates the influence of second order terms on the accuracy of the approximation.

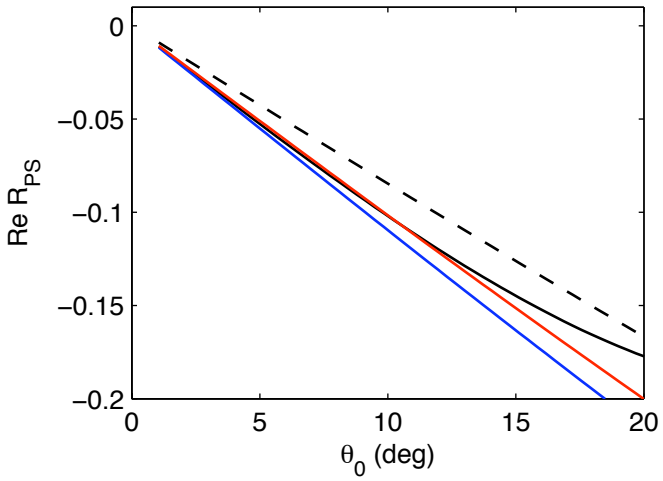

FIG. 7. Comparison of exact $R_{\rm PS}$ (black), linear approximate (dashed), and second order approximate with (red), and without (blue), the terms involving coupling with the target V_P.

Elastic S-wave AVO

This style of analysis may be applied equally straightforwardly to the S-wave problem. Let us do this and gauge the relative importance of various target parameters and their linear and nonlinear influence on reflected amplitudes.

From equation (16) we form

$$R_{\rm SS}(\phi_0) = R^{(1)}_{\rm SS}(\phi_0) + R^{(2)}_{\rm SS}(\phi_0) + ..., \tag{34}$$

where

$$R^{(1)}_{\rm SS}(\phi_0) = \Upsilon_s(\phi_0)a_{VS} + \Upsilon_p(\phi_0)a_{VP} + \Upsilon_\rho(\phi_0)a_\rho, \tag{35}$$

and

$$\begin{aligned} R^{(2)}_{\rm SS}(\phi_0) = \Upsilon_{ss}(\phi_0)a^2_{VS} + \Upsilon_{s\rho}(\phi_0)a_{VS}a_\rho + \Upsilon_{sp}(\phi_0)a_{VS}a_{VP} \\ + \Upsilon_{\rho\rho}(\phi_0)a^2_\rho + \Upsilon_{\rho p}(\phi_0)a_\rho a_{VP} + \Upsilon_{pp}(\phi_0)a^2_{VP}, \end{aligned} \tag{36}$$

etc., and

$$\begin{aligned} &\Upsilon_s(\phi_0) = -\frac{1}{4} + \frac{7}{4}\sin^2\phi_0, \quad \Upsilon_\rho(\phi_0) = -\frac{1}{2} + 2\sin^2\phi_0, \quad \Upsilon_p(\phi_0) = 0, \\ &\Upsilon_{ss}(\phi_0) = -\frac{1}{8} - \left(B - \frac{7}{4}\right)\sin^2\phi_0, \quad \Upsilon_{s\rho}(\phi_0) = (1-2B)\sin^2\phi_0, \quad \Upsilon_{sp}(\phi_0) = 0, \\ &\Upsilon_{\rho\rho}(\phi_0) = -\frac{1}{4} + \left(1 + \frac{1}{4}B' - B\right)\sin^2\phi_0, \quad \Upsilon_{\rho p}(\phi_0) = 0, \quad \Upsilon_{pp}(\phi_0) = 0. \end{aligned} \tag{37}$$

Let us consider first the importance of the second order corrections contained in $R^{(2)}_{\rm SS}(\phi_0)$. In Figure 9 the linear approximation (a–b, in blue) is compared to the second order correction (c–d, in red) with the exact coefficient in black. Evidently there do exist contrast types for which the nonlinear corrections increase the accuracy of the approximation significantly.

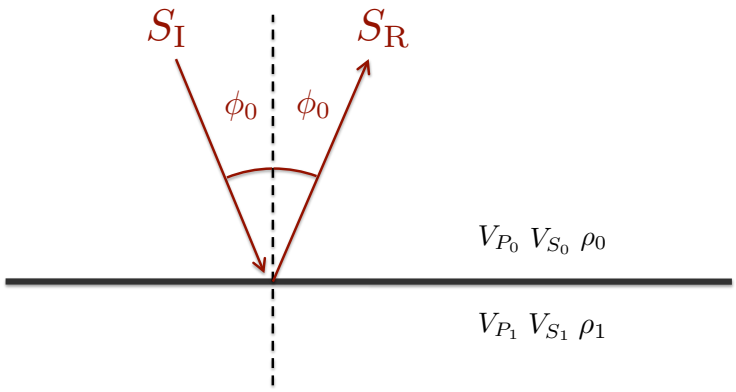

FIG. 8. Incidence/target medium configuration for an elastic S-S AVO problem.

Next, let us consider the relative importance of different components of the second order correction. In particular, consider the target V_{S_1}, which intuition may lead us to expect (correctly) plays the dominant role. In Figure 10 the same elastic model as used in Figure 9 is reconsidered. In bold black the exact $R_{\rm SS}(\phi_0)$ is plotted vs. the linear approximation (dashed), over the angle ranges $0 - -90°$ (a) and $0 - -25°$ (b). In red the full second order correction is plotted, as is, in blue, the second order correction absent the a^2_{VS} term, the

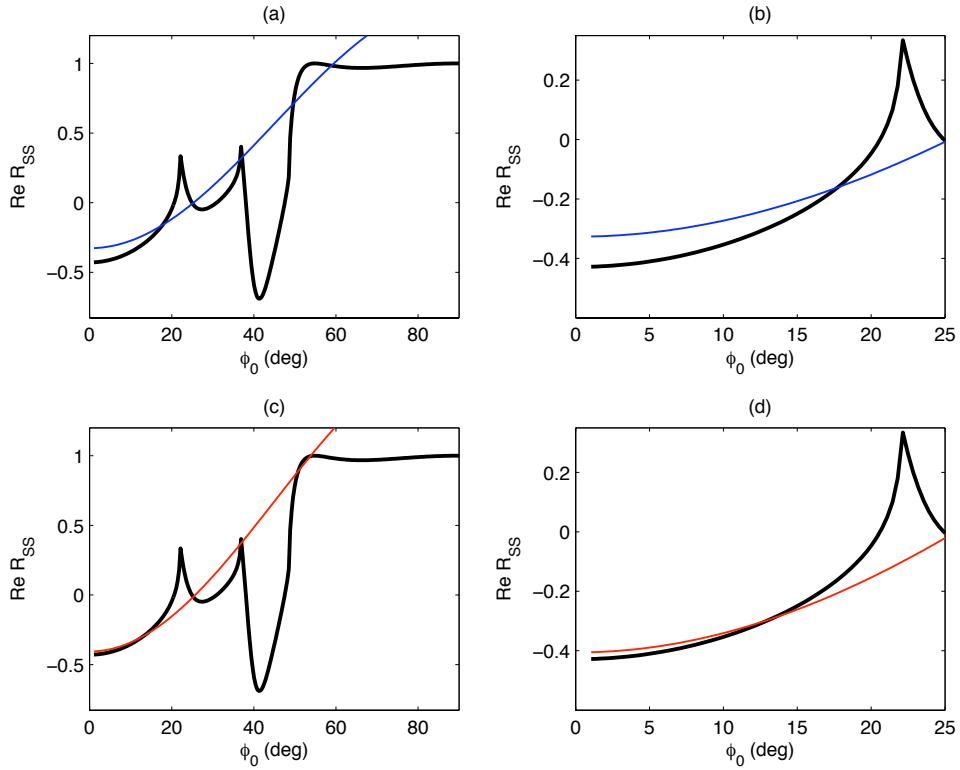

FIG. 9. The importance of 2nd order corrections of $R_{\rm SS}$ for a large contrast target: (a) exact $R_{\rm SS}$ (black) vs. linear approximation (blue) over the full angle range; (b) exact $R_{\rm SS}$ (black) vs. linear approximation (blue) for small angles; (c) exact $R_{\rm SS}$ (black) vs. 2nd order approximation (red) over the full angle range; (b) exact $R_{\rm SS}$ (black) vs. 2nd order approximation (red) for small angles. Incidence medium parameters $V_{P_0} = 2000$m/s, $V_{S_0} = 1500$m/s, $\rho_0 = 2.0$gm/cc; target medium parameters $V_{P_1} = 4000$m/s, $V_{S_1} = 2500$m/s, $\rho_1 = 3.0$gm/cc.

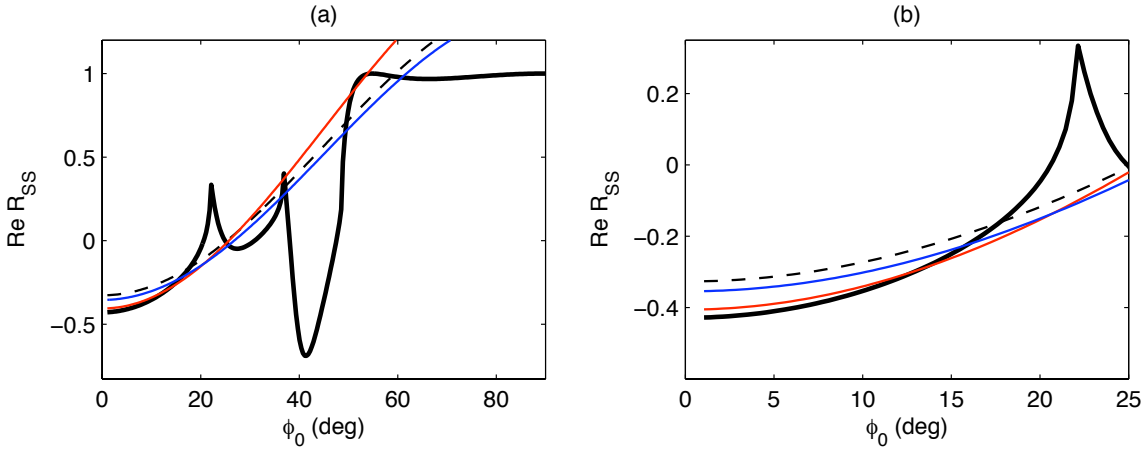

FIG. 10. The importance at 2nd order of the a^2_{VS} term: (a) Four curves over the full angle range: exact $R_{\rm SS}$ (black); linear approximation (dashed); 2nd order approximation (red); and 2nd order approximation without the a^2_{VS} term (blue); (b) same curves for small angles. The 2nd order correction absent the quadratic V_S term is very close to the linear approximation. Medium properties are the same as those in Figure 9.

latter of which does not represent much of an improvement on the original linear approximation.

Finally, let us consider the putatively unimportant target V_{P_1}; notice that all coefficients at first and second order in equations (35)–(37) involving V_{P_1} are zero. Let us once again examine this beginning with the exact $R_{\rm SS}$ for three different target V_P values (see Figure 11a). We see that the reflected S-wave due to an incident S-wave is not independent of target V_P. Nor could it be. Returning briefly to the basic equations, we see in equation (3) that the rightmost column of **S** is

$$-\sqrt{1-(V_{P_1}/V_{S_0})\sin^2\phi_0},$$

signifying that target V_{P_1} will be instrumental in deciding at least one critical angle for $R_{\rm SS}$. Nevertheless, the dependence of $R_{\rm SS}(\phi_0)$ for angles less than this mobile critical angle (seen decreasing from black to blue to red in Figure 11a) on V_{P_1} is so exceedingly weak that a_{VP} appears in its series approximation no earlier than third order. The same $R_{\rm SS}$ approximation, correct to second order, is associated with all three of these models (Figures 11b–d).

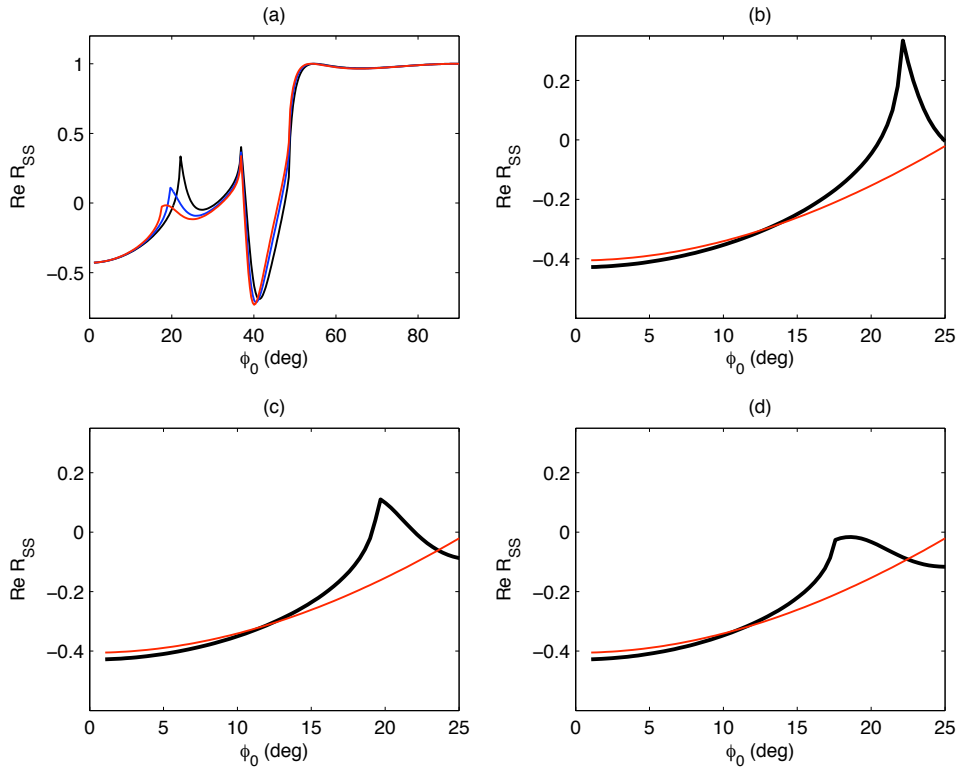

FIG. 11. The importance of target V_P to $R_{\rm SS}$. (a) Three $R_{\rm SS}$ curves, for incidence medium parameters $V_{S_0} = 1500$m/s, $V_{P_0} = 2000$m/s, $\rho_0 = 2.0$gm/cc, and target parameters $V_{S_1} = 2500$m/s, $\rho_1 = 3.0$gm/cc, and three target V_{P_1} values: 4000m/s (black), 4500m/s (blue), and 5000m/s (red). Target V_P alters the $R_{\rm SS}$ curve; however, not only does this alteration not appear in the first order approximation of $R_{\rm SS}$, it also fails to appear in the 2nd order approximation: (b)–(d) the three $R_{\rm SS}$ curves (black) vs. the (unchanging) 2nd order approximation of $R_{\rm SS}$.

Finally, we expand the converted S-P wave amplitude as

$$R_{\rm SP}(\phi_0) = R^{(1)}_{\rm SP}(\phi_0) + R^{(2)}_{\rm SP}(\phi_0) + ..., \tag{38}$$

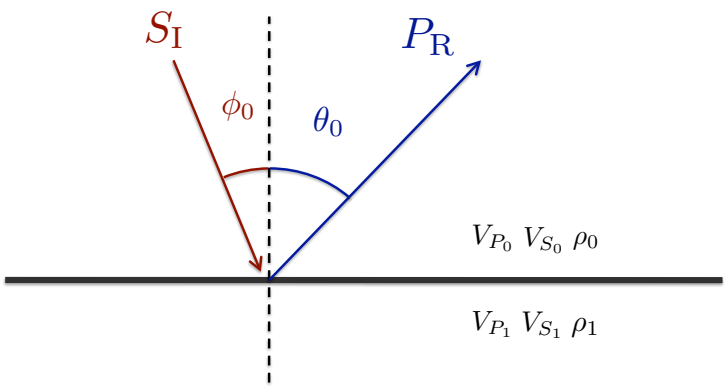

FIG. 12. Incidence/target medium configuration for an elastic S-P AVO problem.

where

$$R_{\rm SP}^{(1)}(\phi_0) = \Omega_s(\phi_0)a_{VS} + \Omega_p(\phi_0)a_{VP} + \Omega_\rho(\phi_0)a_\rho, \tag{39}$$

and

$$\begin{aligned} R_{\rm SP}^{(2)}(\phi_0) = {} & \Omega_{ss}(\phi_0)a_{VS}^2 + \Omega_{s\rho}(\phi_0)a_{VS}a_\rho + \Omega_{sp}(\phi_0)a_{VS}a_{VP} \\ & + \Omega_{\rho\rho}(\phi_0)a_\rho^2 + \Omega_{\rho p}(\phi_0)a_\rho a_{VP} + \Omega_{pp}(\phi_0)a_{VP}^2, \end{aligned} \tag{40}$$

etc., and where

$$\begin{aligned} &\Omega_s(\phi_0) = -B\sin\phi_0, \quad \Omega_\rho(\phi_0) = -\left(B+\frac{1}{2}\right)\sin\phi_0, \quad \Omega_p(\phi_0) = 0, \\ &\Omega_{ss}(\phi_0) = -\frac{3}{4}B\sin\phi_0, \quad \Omega_{s\rho}(\phi_0) = \left(\frac{1}{4}B-\frac{1}{8}\right)\sin\phi_0, \quad \Omega_{sp}(\phi_0) = \frac{1}{4}B\sin\phi_0, \\ &\Omega_{\rho\rho}(\phi_0) = -\frac{1}{2}\sin\phi_0, \quad \Omega_{\rho p}(\phi_0) = \left(\frac{1}{4}B-\frac{1}{8}\right)\sin\phi_0, \quad \Omega_{pp}(\phi_0) = 0. \end{aligned} \tag{41}$$

Here the target V_P regains some of its influence, wherein the coupling between target V_S and ρ at second order is exactly equivalent to the coupling between target V_S and V_P.

Zoeppritz and V_P/V_S ratios of 2

In the foregoing, a curious result is noted. All second order correction terms involving coupling of density with V_P and/or V_S have coefficients containing the term $B - 1/2$. That is, these terms will be identically zero if the incidence medium V_P-V_S ratio is 2, significantly altering the landscape of the nonlinear modeling. This fact may be of particular importance when we discuss the elastic reflection coefficients in terms of *reflectivities* — what this term is saying is that, up to second order, the full elastic reflection coefficients are expressible as the independent sum of density reflectivity and V_P and V_S reflectivities.

ANELASTIC AVO

In this section we examine P-wave, P-S (converted wave) and S-S (shear wave) reflections occurring when a wave in an elastic incidence medium impinges on an anelastic target

medium. In particular, we wish to (1) predict the influence of a sudden strong contrast from a predominantly elastic incidence medium to an anelastic target medium on AVO curves, and (2) generate inverse procedures for determining target Q_P and Q_S values from the AVF behaviour of the resulting reflection strengths.

Equations (1)–(16) must be augmented in order to capture the AVO and AVF behaviour of an anelastic target. In particular, the ratios C, D, E, and F require alteration. As reviewed by Aki and Richards (2002), the elastic velocities must be replaced with expressions involving (1) elastic phase velocities at specified reference frequencies, and (2) P- and S-wave quality factors Q_P and Q_S respectively, which (A) cause the wave to attenuate during propagation and (B) cause the wave to propagate with different velocities at frequencies different from the reference values. In particular we have

$$C = \frac{V_{P_1}}{V_{P_0}}\left[1 - \frac{F_P(\omega)}{Q_{P_1}}\right], \quad F = \frac{V_{S_1}}{V_{S_0}}\left[1 - \frac{F_S(\omega)}{Q_{S_1}}\right], \tag{42}$$

where

$$\begin{aligned} F_P(\omega) &= \frac{i}{2} - \frac{1}{\pi}\log\left(\frac{\omega}{\omega_P}\right) \\ F_S(\omega) &= \frac{i}{2} - \frac{1}{\pi}\log\left(\frac{\omega}{\omega_S}\right), \end{aligned} \tag{43}$$

ω is angular frequency, and ω_P and ω_S are reference frequencies. Equation (42) affects D and E also via equation (10).

Since we have added two additional medium properties to the mix, we must introduce two additional perturbations so that they can be included in the expansions of the augmented Zoeppritz equations. We define

$$\begin{aligned} a_{QP} &= \frac{1}{Q_{P_1}}, \\ a_{QS} &= \frac{1}{Q_{S_1}}, \end{aligned} \tag{44}$$

upon which, using equation (8), the new ratios become

$$\begin{aligned} C &= (1 - a_{VP})^{1/2}[1 - F_P(\omega)a_{QP}] \\ F &= (1 - a_{VS})^{1/2}[1 - F_S(\omega)a_{QS}] \\ D &= B(1 - a_{VS})^{1/2}[1 - F_S(\omega)a_{QS}] \\ E &= B'(1 - a_{VP})^{1/2}[1 - F_P(\omega)a_{QP}]. \end{aligned} \tag{45}$$

These may now be expanded in series, taking the place of the series in equations (9)–(10), and anelastic versions of any of R_{PP}, R_{PS}, R_{SS} or R_{SP} can be examined.

Anelastic P-P AVO

We next expand R_{PP} for incidence/target media as illustrated in Figure 13. Substituting equations (23) into the equations (12)–(16) leads to an anelastic P-P wave reflection

coefficient of

$$R_{\rm PP}(\theta_0,\omega) = R^{(1)}_{\rm PP}(\theta_0,\omega) + R^{(2)}_{\rm PP}(\theta_0,\omega) + ..., \tag{46}$$

where

$$R^{(1)}_{\rm PP}(\theta_0,\omega) = \Delta'_p a_{VP} + \Delta'_s a_{VS} + \Delta'_\rho a_\rho + \Delta'_{Q_p} a_{QP} + \Delta'_{Q_s} a_{QS}, \tag{47}$$

and

$$\begin{aligned} R^{(2)}_{\rm PP}(\theta_0,\omega) = {} & \Delta'_{pp} a^2_{VP} + \Delta'_{ps} a_{VP} a_{VS} + \Delta'_{p\rho} a_{VP} a_\rho + \Delta'_{pQp} a_{VP} a_{QP} \\ & + \Delta'_{pQs} a_{VP} a_{QS} + \Delta'_{ss} a^2_{VS} + \Delta'_{s\rho} a_{VS} a_\rho + \Delta'_{sQp} a_{VS} a_{QP} \\ & + \Delta'_{sQs} a_{VS} a_{QS} + \Delta'_{\rho\rho} a^2_\rho + \Delta'_{\rho Qp} a_\rho a_{QP} + \Delta'_{\rho Qs} a_\rho a_{QS} + \Delta'_{QpQp} a^2_{QP} \\ & + \Delta'_{QsQp} a_{QP} a_{QS} + \Delta'_{QsQs} a^2_{QS}, \end{aligned} \tag{48}$$

etc., and where the coefficients of the first order terms are

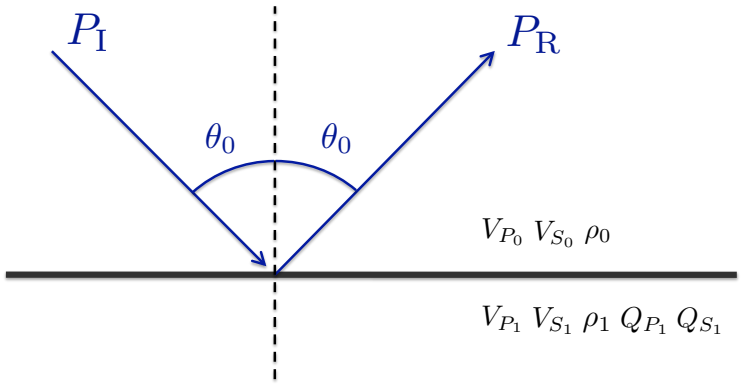

FIG. 13. Incidence/target medium properties for a P-P anelastic AVO problem.

$$\Delta'_p(\theta_0) = \frac{1}{4}\left(1+\sin^2\theta_0\right), \quad \Delta'_s(\theta_0) = -2B^2\sin^2\theta_0,$$

$$\Delta'_\rho(\theta_0) = \frac{1}{2}\left(1-4B^2\sin^2\theta_0\right), \quad \Delta'_{Qp}(\theta_0,\omega) = -\frac{1}{2}F_P(\omega)\left(1+\sin^2\theta_0\right),$$

$$\Delta'_{Q_s}(\theta_0,\omega) = 4B^2F_S(\omega)\sin^2\theta_0,$$

and the coefficients of the second order terms are

$$\Delta'_{pp}(\theta_0) = \left(\frac{1}{8}+\frac{1}{4}\sin^2\theta_0\right), \quad \Delta'_{ps}(\theta_0) = 0, \quad \Delta'_{p\rho}(\theta_0) = 0,$$

$$\Delta'_{pQp}(\theta_0,\omega) = -\frac{1}{2}F_P(\omega)\sin^2\theta_0, \quad \Delta'_{pQs}(\theta_0,\omega) = 0, \quad \Delta'_{ss}(\theta_0) = B^2(B-2)\sin^2\theta_0,$$

$$\Delta'_{s\rho}(\theta_0) = B^2(2B-1)\sin^2\theta_0, \quad \Delta'_{sQp}(\theta_0,\omega) = 0, \quad \Delta'_{sQs}(\theta_0,\omega) = 4B^2(1-B)F_S(\omega)\sin^2\theta_0$$

$$\Delta'_{\rho\rho}(\theta_0) = \frac{1}{4} - B\left(\frac{1}{4}+B-B^2\right)\sin^2\theta_0, \quad \Delta'_{\rho Qp}(\theta_0,\omega) = 0,$$

$$\Delta'_{\rho Qs}(\theta_0,\omega) = 2B^2(1-2B)F_S(\omega)\sin^2\theta_0, \quad \Delta'_{QpQp}(\theta_0,\omega) = -\frac{1}{4}\left(1+\sin^2\theta_0\right)F_P^2(\omega),$$
$$\Delta'_{QpQs}(\theta_0,\omega) = 0, \quad \Delta'_{QsQs}(\theta_0,\omega) = -2B^2(1-2B)F_S^2(\omega)\sin^2\theta_0.$$

Consider the linear approximation $R_{\rm PP}(\theta_0,\omega) \approx R^{(1)}_{\rm PP}(\theta_0,\omega)$. In Figure 14a, we plot the real part of the exact anelastic $R_{\rm PP}$ for a small range of angles at three representative frequencies. How important it is, for targets of these types, for us to include the two anelastic terms at first order in a_{QP} and a_{QS}, is visible in Figures 14b–d, in which the blue curves represent the correct linear approximations, and the red curves represent the AVO response that would be modelled using the correct elastic coefficients but neglecting to correct for anelasticity. Specifically, the blue curves are produced with the formula

$$R_{\rm PP}(\theta_0,\omega) \approx \Delta'_p a_{VP} + \Delta'_s a_{VS} + \Delta'_\rho a_\rho + \Delta'_{Q_p} a_{QP} + \Delta'_{Q_s} a_{QS}, \tag{49}$$

and the red curve with the fomula

$$R_{\rm PP}(\theta_0,\omega) \approx \Delta'_p a_{VP} + \Delta'_s a_{VS} + \Delta'_\rho a_\rho. \tag{50}$$

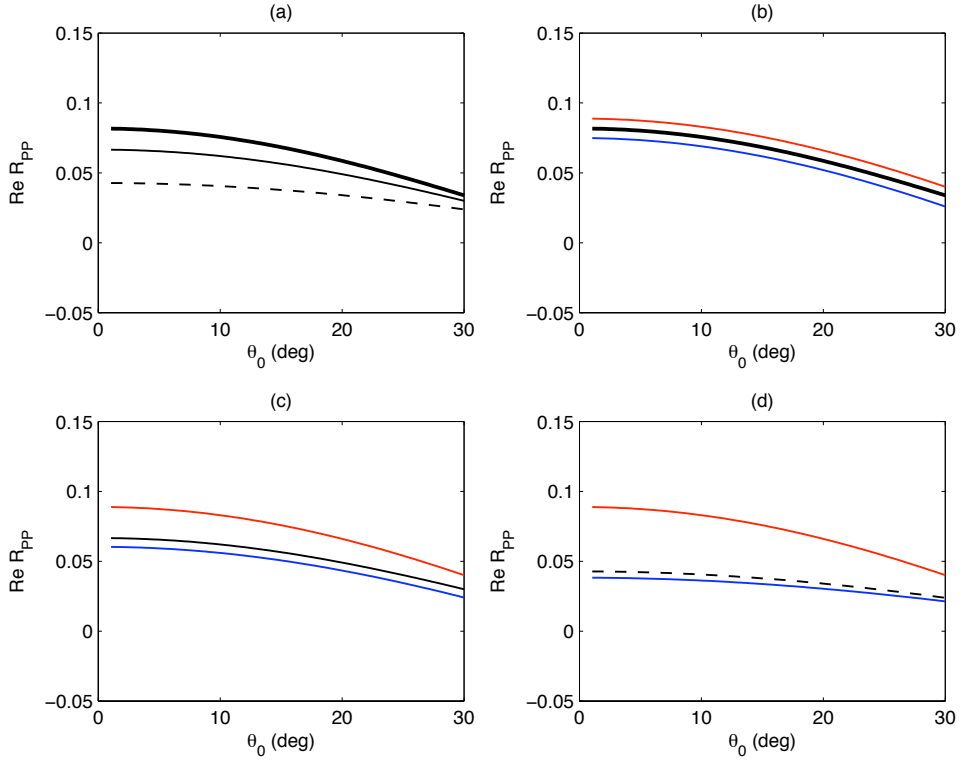

FIG. 14. Importance of inclusion of Q correction terms at first order for small contrast. (a) Three exact anelastic $R_{\rm PP}$ AVO curves for incidence medium parameters $V_{P_0} = 2000$m/s, $V_{S_0} = 1500$m/s, $\rho_0 = 2.0$gm/cc, and target medium parameters $V_{P_1} = 2200$m/s, $V_{S_0} = 1600$m/s, $\rho_0 = 2.2$gm/cc, $Q_{P_1} = 10$, and $Q_{S_1} = 10$, at fixed frequencies 50 Hz (bold), 20 Hz (solid), and 5 Hz (dashed). (b)–(d) Each of the three exact AVO curves compared against linear approximations with (blue) and without (red) the linear anelastic correction terms.

Next we examine the importance of the second order corrections to anelastic $R_{\rm PP}$ for large contrasts. In Figure 15a the real part of the exact $R_{\rm PP}(\theta_0,\omega)$ is plotted for thee same

three representative frequencies as in Figure 14, but for a larger contrast target. In the remaining three plots (Figures 15b–d), these three curves are approximated linearly (blue) and with second order corrections (red). In all cases the addition of on extra order leads to significant increase in approximation accuracy over the angle range of practical applicability to AVO.

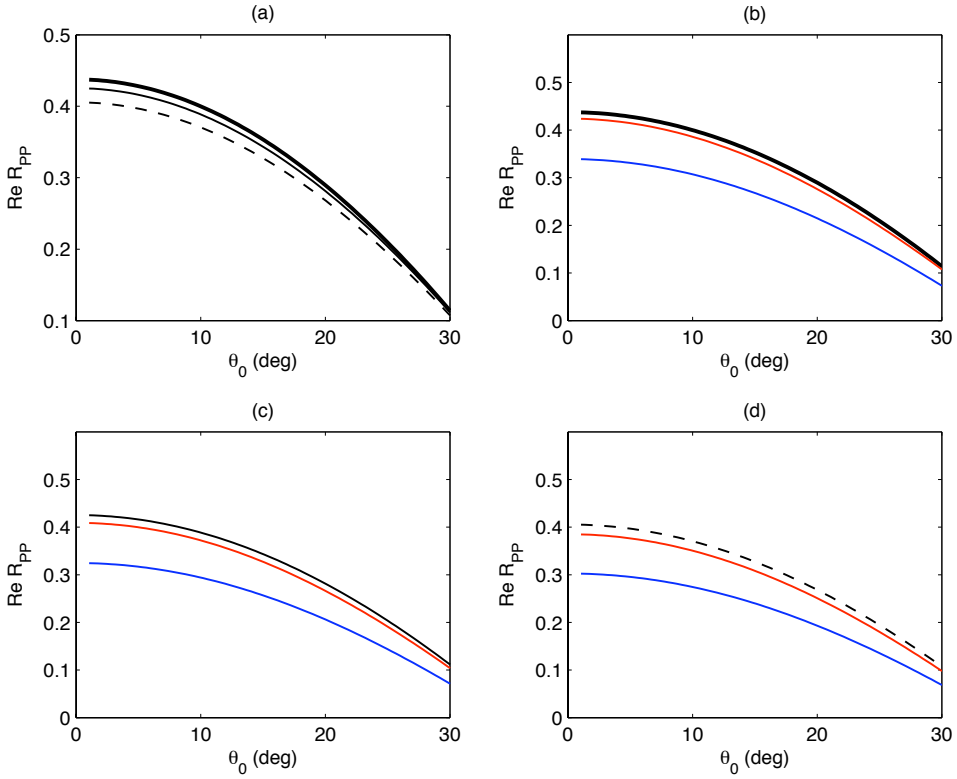

FIG. 15. Importance of second order corrections at large contrast. (a) Three exact anelastic $R_{\rm PP}$ AVO curves for incidence medium parameters $V_{P_0} = 2000$m/s, $V_{S_0} = 1500$m/s, $\rho_0 = 2.0$gm/cc, and target medium parameters $V_{P_1} = 3000$m/s, $V_{S_0} = 2500$m/s, $\rho_0 = 3.5$gm/cc, $Q_{P_1} = 10$, and $Q_{S_1} = 10$, at fixed frequencies 50 Hz (bold), 20 Hz (solid), and 5 Hz (dashed). (b)–(d) Each of the three exact AVO curves compared against linear approximations (blue) and second order approximations (red).

Anelastic converted wave AVO and AVF

We next expand $R_{\rm PS}$ for incidence/target media as illustrated in Figure 16. Substituting equations (23) into the equations (12)–(16) leads to an anelastic converted wave reflection coefficient of

$$R_{\rm PS}(\theta_0,\omega) = R^{(1)}_{\rm PS}(\theta_0,\omega) + R^{(2)}_{\rm PS}(\theta_0,\omega) + ..., \tag{51}$$

where

$$R^{(1)}_{\rm PS}(\theta_0,\omega) = \Lambda'_s a_{VS} + \Lambda'_s a_{VS} + \Lambda'_\rho a_\rho + \Lambda'_{Q_p} a_{QP} + \Lambda'_{Q_s} a_{QS} \tag{52}$$

and

$$\begin{aligned} R_{\rm PS}^{(2)}(\theta_0,\omega) = &\Lambda'_{pp}a_{VP}^2 + \Lambda'_{ps}a_{VP}a_{VS} + \Lambda'_{p\rho}a_{VP}a_\rho + \Lambda'_{pQp}a_{VP}a_{QS} \\ &+ \Lambda'_{pQs}a_{VP}a_{QS} + \Lambda'_{ss}a_{VS}^2 + \Lambda'_{s\rho}a_{VS}a_\rho + \Lambda'_{sQp}a_{VS}a_{QS} \\ &+ \Lambda'_{sQs}a_{VS}a_{QS} + \Lambda'_{\rho\rho}a_\rho^2 + \Lambda'_{\rho Qp}a_\rho a_{QP} + \Lambda'_{\rho Qs}a_\rho a_{QS} \\ &+ \Lambda'_{QpQp}a_{QP}^2 + \Lambda'_{QpQs}a_{QP}a_{QS} + \Lambda'_{QsQs}a_{QS}^2, \end{aligned} \tag{53}$$

etc., where the linear coefficients are

$$\Lambda'_p = 0, \quad \Lambda'_s(\theta_0) = -B\sin\theta_0, \quad \Lambda'_\rho(\theta_0) = -\left(B - \frac{1}{2}\right)\sin\theta_0,$$

and

$$\Lambda'_{Q_p}(\theta_0,\omega) = 0, \quad \Lambda'_{Q_s}(\theta_0,\omega) = 2BF_S(\omega)\sin\theta_0,$$

the the second order coefficients are

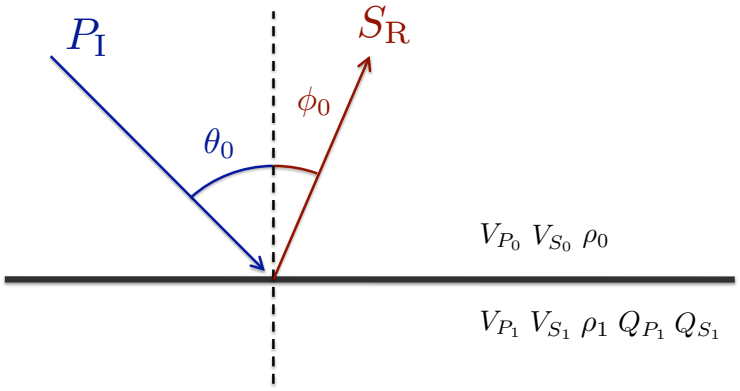

FIG. 16. Incidence/target medium properties for a converted wave anelastic AVO problem.

$$\Lambda'_{pp}(\theta_0) = 0, \quad \Lambda'_{ps}(\theta_0) = \frac{1}{4}B\sin\theta_0,$$

$$\Lambda'_{p\rho}(\theta_0) = -\frac{1}{8}(1-2B)\sin\theta_0, \quad \Lambda'_{pQp}(\theta_0,\omega) = 0,$$

$$\Lambda'_{pQs}(\theta_0,\omega) = -\frac{1}{2}BF_S(\omega)\sin\theta_0, \quad \Lambda'_{ss}(\theta_0) = -\frac{3}{4}B\sin\theta_0,$$

$$\Lambda'_{s\rho}(\theta_0) = -\frac{1}{8}(1-2B)\sin\theta_0, \quad \Lambda'_{sQp}(\theta_0,\omega) = -\frac{1}{2}BF_P(\omega)\sin\theta_0,$$

$$\Lambda'_{sQs}(\theta_0,\omega) = BF_S(\omega)\sin\theta_0, \quad \Lambda'_{\rho\rho}(\theta_0) = -\frac{1}{2}\sin\theta_0,$$

$$\Lambda'_{\rho Qp}(\theta_0,\omega) = \frac{1}{4}(1-2B)F_P(\omega)\sin\theta_0, \quad \Lambda'_{\rho Qs}(\theta_0,\omega) = \frac{1}{4}(1-2B)F_S(\omega)\sin\theta_0,$$

$$\Lambda'_{QpQp}(\theta_0,\omega) = 0, \quad \Lambda'_{QpQs}(\theta_0,\omega) = BF_P(\omega)F_S(\omega)\sin\theta_0,$$

and

$$\Lambda'_{QsQs}(\theta_0, \omega) = 0.$$

To first order, then, we have

$$R_{\rm PS}(\theta_0, \omega) \approx -B \sin\theta_0 \; a_{VS} - \left(B - \frac{1}{2}\right) \sin\theta_0 \; a_\rho + 2BF_S(\omega) \sin\theta_0 \; a_{QS}. \tag{54}$$

Let us examine both the frequency dependence of the AVO response of $R_{\rm PS}$, and the AVF behaviour explicitly (recalling the discussion around Figure 2). We have seen that the approximations at first and second order are accurate around angles that do not approach critical, so let us confine our attention to these regions. In Figure 17a–c we display sets of five AVO curves for $R_{\rm PS}$ from a single target at five representative frequencies. Figures

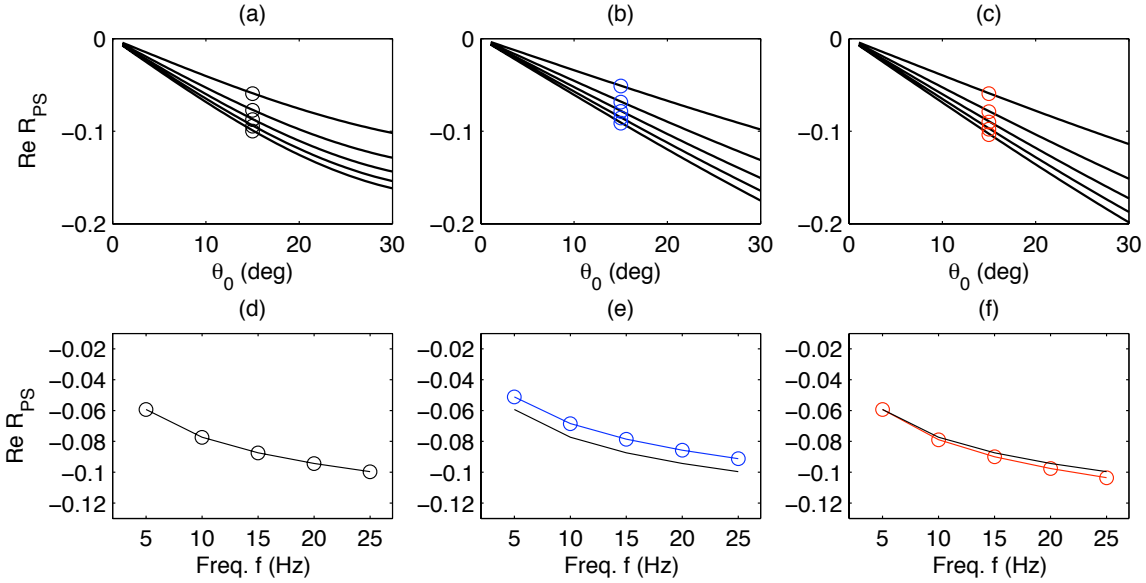

FIG. 17. Real part of $R_{\rm PS}$ and its angle and frequency variations. (a) Exact $R_{\rm PS}$ vs. angle for fixed frequencies 5 Hz, 10Hz, 15 Hz, 20 Hz and 25 Hz, with values marked off at a representative angle $\theta_0 = 15°$. (b) As (a) but using linearized $R_{\rm PS}$ approximation. (c) As (a) but using second order corrected $R_{\rm PS}$ approximation. (d) $R_{\rm PS}$ values picked from (a) at $\theta_0 = 15°$ and plotted vs. frequency. (e) As (d) but picking from linear approximation; Incidence medium parameters $V_{P_0} = 2000$m/s, $V_{S_0} = 1500$m/s, $\rho_0 = 2.0$gm/cc, and target medium parameters $V_{P_1} = 2200$m/s, $V_{S_0} = 1700$m/s, $\rho_0 = 2.5$gm/cc, $Q_{P_1} = 5$, and $Q_{S_1} = 5$.

17a–c are concerned with AVO altered to account for frequency dependence. Let us next examine the same quantities, $R_{\rm PS}$, explicitly in terms of AVF. In Figures 17a–c we have indicated with circles points on the AVO curves corresponding to a fixed angle $\theta_0 = 15°$. In Figures 17d–f we extract these sets of five points from the $R_{\rm PS}$ data and plot them vs. frequency. In (d) we show in black the exact values, and in (e)–(f) we show the linear and second order approximations in blue and red respectively plotted in comparison to the exact.

We note that the second order correction is of some significance in increasing the accuracy of the approximation for these contrasts. However, we also note that the error in the linear approximation is close to being an additive constant—the curvature of $R_{\rm PS}(\theta_0 = 15°, \omega)$ vs. $f = \omega/2\pi$ is captured by $R^{(1)}_{\rm PS}$ fairly well.

Mode conversions from Q_S and Q_P contrasts

Contrasts in a single parameter only, the quality factor, across an otherwise transparent boundary (i.e., across which the elastic impedance remains constant) are known in theory (e.g., Lines et al., 2008) and in laboratory experiments (Lines et al., 2011b) to cause reflections. With the expansion of R_{PS} in equation (57), we may draw some conclusions about a related process, P-S mode conversions from quality factor contrasts.

Consider the coefficients in equations (58)–(59). In particular, we see that

$$\Lambda'_{Qp} = 0, \quad \Lambda'_{Qs} \neq 0, \tag{55}$$

and

$$\Lambda'_{QpQp} = 0, \quad \Lambda'_{QpQs} \neq 0, \quad \Lambda'_{QsQs} = 0. \tag{56}$$

If either of Q_P and/or Q_S vary from infinite in the incidence medium to low finite values in the target medium, but all the other parameters are invariant across the boundary, so that $a_{VP} = a_{VS} = a_\rho = 0$, then

$$R_{\text{PS}}(\theta_0, \omega) = R^{(1)}_{\text{PS}}(\theta_0, \omega) + R^{(2)}_{\text{PS}}(\theta_0, \omega) + ..., \tag{57}$$

where

$$R^{(1)}_{\text{PS}}(\theta_0, \omega) = \Lambda'_{Q_s} a_{QS} \tag{58}$$

and

$$R^{(2)}_{\text{PS}}(\theta_0, \omega) = \Lambda'_{QpQs} a_{QP} a_{QS}. \tag{59}$$

Hence, to first order,

1. A contrast in Q_S alone causes a P-S mode conversion which propagates thereafter as an elastic wave;
2. A contrast in Q_P does not.

At second order there is no change in these conclusions. Therefore target Q_P variations alone produce mode conversions of negligible (third order or higher) strength for small and moderate angles.

However, if a Q_S and Q_P variation occur simultaneously across the otherwise transparent boundary, then the Q_P value does influence the strength of the P-S mode conversion at second order, hence nonnegligibly for small and moderate angles. In practice, Q_S alterations in the total absence of Q_P variations are unlikely for continuum mechanical reasons, as discussed by Waters (1978). Since the origins of Q_S are associated with a complex, frequency dependent shear modulus, a non-complex P-wave modulus $\kappa + (4/3)\mu$ with a complex shear modulus is unlikely. Therefore our conclusions about simultaneous Q_P and Q_S contrasts may carry more practical geophysical importance.

Anelastic inversion I

We can exemplify the direct inversion regimen discussed in equations (17)–(27) by inverting converted wave anelastic reflection amplitude data to estimate the target Q_S, using variability in frequency rather than angle to render the problem tractable. We will work within the linear approximation. Before applying the formulation for all available frequencies (in this case all five data points plotted in Figures 17d–f), we may make a foray into the problem using only two frequencies, $f_1 = \omega_1/2\pi = 5$Hz and $f_2 = \omega_2/2\pi = 10$Hz. Evaluating equation (54) twice, once for each frequency, and subtracting, we eliminate contributions to $R_{\rm PS}$ from a_{VS} and a_ρ, and may solve for a_{Q_S} thus:

$$a_{Q_S} \approx \frac{1}{2B\sin\theta_0}\frac{R_{\rm PS}(\theta_0,\omega_1) - R_{\rm PS}(\theta_0,\omega_2)}{F_S(\omega_1) - F_S(\omega_2)}, \tag{60}$$

which, when the actual values of the converted wave reflection amplitudes are used generates an estimate of $Q_S = 5.1$, which is within %2 of the correct value.

Following the prescription for N input frequencies we can form the matrix equation

$$\mathbf{A}_{PS}\begin{bmatrix} a_{VS} \\ a_\rho \\ a_{QS} \end{bmatrix} = \mathbf{r}_{PS}, \tag{61}$$

where

$$\mathbf{A}_{PS} = 2B\sin\theta_0\begin{bmatrix} -\frac{1}{2} & -\frac{1}{2}\left(1-\frac{1}{2B}\right) & F_S(\omega_1) \\ -\frac{1}{2} & -\frac{1}{2}\left(1-\frac{1}{2B}\right) & F_S(\omega_2) \\ \vdots & \vdots & \vdots \\ -\frac{1}{2} & -\frac{1}{2}\left(1-\frac{1}{2B}\right) & F_S(\omega_N) \end{bmatrix}, \tag{62}$$

and

$$\mathbf{r}_{PS} = \begin{bmatrix} R_{\rm PS}(\theta_0,\omega_1) \\ R_{\rm PS}(\theta_0,\omega_2) \\ \vdots \\ R_{\rm PS}(\theta_0,\omega_N) \end{bmatrix}. \tag{63}$$

This may be solved for the optimum perturbation vector $[a_{VS}, a_\rho, a_{QS}]^T$ in the least squares sense as

$$\begin{bmatrix} a_{VS} \\ a_\rho \\ a_{QS} \end{bmatrix}_{\rm LSQ} = \left(\mathbf{A}_{PS}^H\mathbf{A}_{PS}\right)^{-1}\mathbf{A}_{PS}^H\mathbf{r}_{PS}, \tag{64}$$

which, when all five of the frequencies plotted in Figure 17d–f are included recovers a target quality factor of $Q_S = 4.96$, which is within %4 of the correct value. These error ranges are in keeping with a linear approximation for targets with large contrasts in quality factors (Innanen, 2011a).

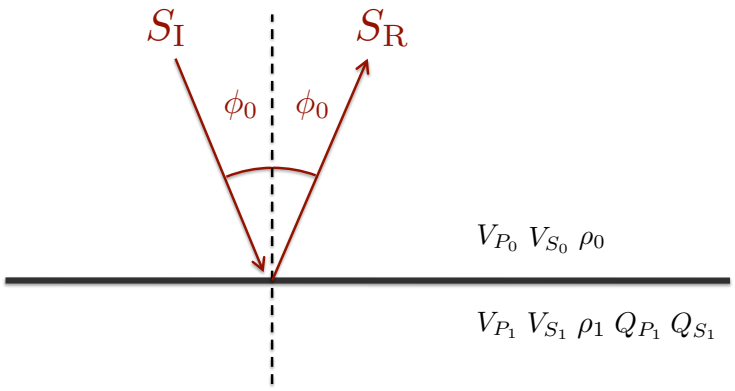

FIG. 18. Incidence/target medium properties for a P-P anelastic AVO problem.

Anelastic inversion II

Let us consider the problems in slightly greater detail. Beginning again with the coefficients for the expansion of anelastic $R_{\rm PP}$, i.e., the Δ quantities in

$$\begin{aligned} R_{\rm PP}(\theta_0,\omega) =& \Delta_p(\theta_0)a_{VP} + \Delta_s(\theta_0)a_{VS} + \Delta_\rho(\theta_0)a_\rho \\ &+ \Delta_{Q_p}(\theta_0,\omega)a_{QP} + \Delta_{Q_s}(\theta_0,\omega)a_{QS}. \end{aligned} \tag{65}$$

Since our interest is in determining target Q_P and Q_S, we may immediately simplify matters and eliminate the other parameters by considering only differences of $R_{\rm PP}$ across frequencies. In fact

$$\delta R_{\rm PP}(\theta_0,\omega_1,\omega_2) = \delta\Delta_{Q_p}(\theta_0,\omega_1,\omega_2)a_{QP} + \delta\Delta_{Q_s}(\theta_0,\omega_1,\omega_2)a_{QS}, \tag{66}$$

where

$$\delta R_{\rm PP}(\theta_0,\omega_1,\omega_2) = R_{\rm PP}(\theta_0,\omega_1) - R_{\rm PP}(\theta_0,\omega_2), \tag{67}$$

and

$$\begin{aligned} \delta\Delta_{Q_p}(\theta_0,\omega_1,\omega_2) &= \Delta_{Q_p}(\theta_0,\omega_1) - \Delta_{Q_p}(\theta_0,\omega_2) \\ \delta\Delta_{Q_s}(\theta_0,\omega_1,\omega_2) &= \Delta_{Q_s}(\theta_0,\omega_1) - \Delta_{Q_s}(\theta_0,\omega_2). \end{aligned} \tag{68}$$

In Figures 19 and 20 we consider the input, and then the recovery of the two quality factors from the frequency dependence of $R_{\rm PP}$. Figures 20c-d indicate that even in the linear approximation the P-wave quality factor is reconstructed within a very low error, but that the Q_S recovery is very poor; in fact, regardless of which fixed angle is used the S-wave quality factor perturbation is very close to zero. Hence the $R_{\rm PP}$ mode may be best suited for recovery of Q_P.

We can repeat the above analysis for the $R_{\rm PS}$ mode. Again, we begin with the standard expansion

$$R_{\rm PS}(\theta_0,\omega) = \Lambda_s(\theta_0)a_{VS} + \Lambda_\rho(\theta_0)a_\rho + \Lambda_{Q_s}(\theta_0,\omega)a_{QS}. \tag{69}$$

This time differencing of the reflection data over frequencies leaves only one perturbation, a_{QS}. In fact

$$a_{QS}(\omega_1,\omega_2) = \frac{\delta R_{\rm PS}(\theta_0,\omega_1,\omega_2)}{\delta \Lambda_{Q_s}(\theta_0,\omega_1,\omega_2)}, \tag{70}$$

where

$$\delta R_{\rm PS}(\theta_0,\omega_1,\omega_2) = R_{\rm PS}(\theta_0,\omega_1) - R_{\rm PS}(\theta_0,\omega_2), \tag{71}$$

and

$$\delta \Lambda_{Q_s}(\theta_0,\omega_1,\omega_2) = \Lambda_{Q_s}(\theta_0,\omega_1) - \Lambda_{Q_s}(\theta_0,\omega_2). \tag{72}$$

Equation (70) allows us to discuss the perturbation a_{QS} in terms of the rate of change of $R_{\rm PS}$ with frequency. Since

$$\begin{aligned}
\delta \Lambda_{Q_s}(\theta_0,\omega_1,\omega_2) &= 2B \sin_0[F_S(\omega_1) - F_S(\omega_2)] \\
&= \frac{2B}{\pi} \sin\theta_0 \left[\log\left(\frac{\omega_1}{\omega_S}\right) - \log\left(\frac{\omega_2}{\omega_S}\right)\right] \\
&= \frac{2B}{\pi} \sin\theta_0 [\log\omega_1 - \log\omega_2] \\
&= \frac{2B}{\pi} \sin\theta_0 \ \delta\log\omega \\
&= \frac{2B}{\pi} \sin\theta_0 \frac{\delta\omega}{\omega},
\end{aligned} \tag{73}$$

we may re-write equation (70) as

$$a_{QS} \approx \left(\frac{\pi}{2} \times \frac{V_{P_0}}{V_{S_0}} \times \frac{\omega}{\sin\theta_0}\right) \times \frac{\delta R_{\rm PS}}{\delta\omega}. \tag{74}$$

The Q_S perturbation, then, is evidently proportional to the rate of change of $R_{\rm PS}$ with frequency.

In Figures 21, 22 and 23 some numerical examples of the recovery of Q_S and Q_P are illustrated. This time we note the opposite of the $R_{\rm PP}$ case; Q_P is (obviously) not determined, but Q_S is with high accuracy, for both pairs of frequencies considered and regardless of which fixed incidence angle is used.

Anelastic S-wave AVO and AVF

Analysis for anelastic S-wave AVO and AVF (see the configuration illustrated in Figure 18) proceeds similarly. We expand $R_{\rm SS}$ as

$$R_{\rm SS}(\phi_0,\omega) = R^{(1)}_{\rm SS}(\phi_0,\omega) + R^{(2)}_{\rm SS}(\phi_0,\omega) + ..., \tag{75}$$

where

$$R^{(1)}_{\rm SS}(\phi_0) = \Upsilon'_s a_{VS} + \Upsilon'_p a_{VP} + \Upsilon'_\rho a_\rho + \Upsilon'_{Q_s} a_{QS} + \Upsilon'_{Q_p} a_{QP}, \tag{76}$$

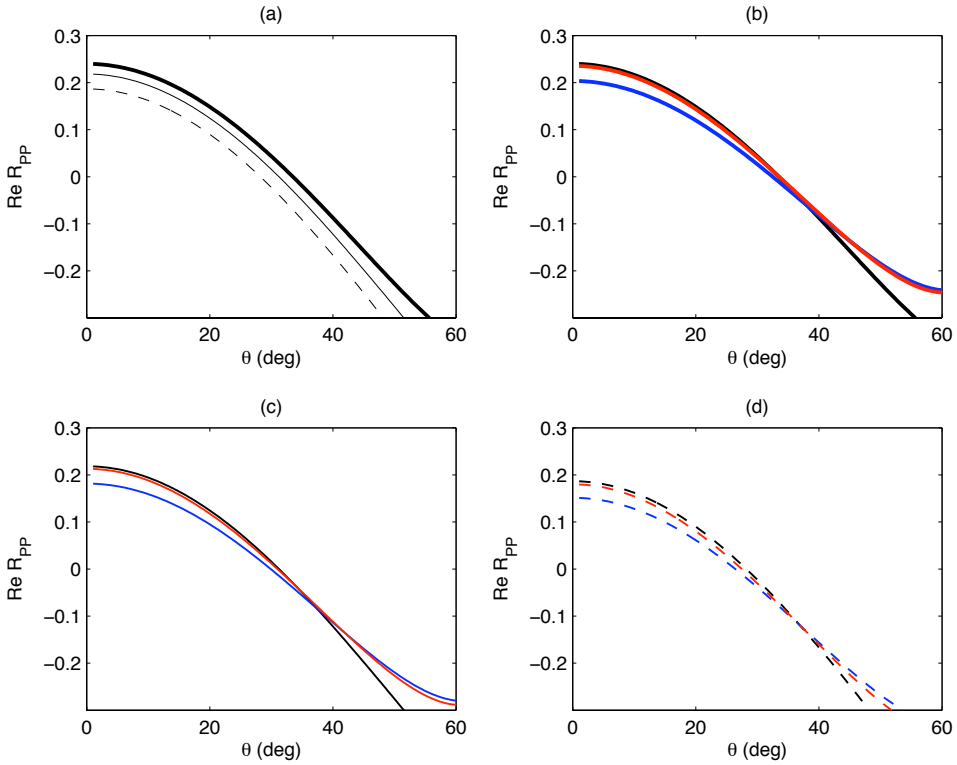

FIG. 19. Input R_{PP} curves for anelastic inversion: first order (blue), second order (red) vs. exact (black). (a) R_{PP} at three representative frequencies. (b)–(d) 1st, 2nd order, and exact coefficients at each frequency.

and

$$\begin{aligned} R^{(2)}_{\mathrm{SS}}(\phi_0) =& \Upsilon'_{ss}a^2_{VS} + \Upsilon'_{s\rho}a_{VS}a_{\rho} + \Upsilon'_{sp}a_{VS}a_{VP} + \Upsilon'_{sQs}a_{VS}a_{QS} + \Upsilon'_{sQp}a_{VS}a_{QP} \\ &+ \Upsilon'_{\rho\rho}a^2_{\rho} + \Upsilon'_{\rho p}a_{\rho}a_{VP} + \Upsilon'_{\rho Qs}a_{\rho}a_{QS} + \Upsilon'_{\rho Qp}a_{\rho}a_{QP} + \Upsilon'_{pp}a^2_{VP} \\ &+ \Upsilon'_{pQs}a_{VP}a_{QS} + \Upsilon'_{pQp}a_{VP}a_{QP} + \Upsilon'_{QsQs}a^2_{QS} + \Upsilon'_{QsQp}a_{QS}a_{QP} \\ &+ \Upsilon'_{QpQp}a^2_{QP} \end{aligned} \tag{77}$$

etc., and

$$\Upsilon'_{s}(\phi_0) = -\frac{1}{4} + \frac{7}{4}\sin^2\phi_0, \quad \Upsilon'_{\rho}(\phi_0) = -\frac{1}{2} + 2\sin^2\phi_0, \quad \Upsilon'_{p}(\phi_0) = 0,$$

$$\Upsilon'_{Qs}(\phi_0,\omega) = \frac{1}{2}F_S(\omega) - \frac{7}{2}F_S(\omega)\sin^2\phi_0, \quad \Upsilon'_{Qp}(\phi_0,\omega) = 0,$$

$$\Upsilon'_{ss}(\phi_0) = -\frac{1}{8} - \left(B - \frac{7}{4}\right)\sin^2\phi_0, \quad \Upsilon'_{s\rho}(\phi_0) = (1-2B)\sin^2\phi_0, \quad \Upsilon'_{sp}(\phi_0) = 0,$$

$$\Upsilon'_{sQs}(\phi_0,\omega) = \left(4B - \frac{7}{2}\right)F_S(\omega)\sin^2\phi_0, \quad \Upsilon'_{sQp}(\phi_0,\omega) = 0,$$

$$\Upsilon'_{\rho\rho}(\phi_0) = -\frac{1}{4} + \left(1 + \frac{1}{4}B' - B\right)\sin^2\phi_0, \quad \Upsilon'_{pp}(\phi_0) = 0,$$

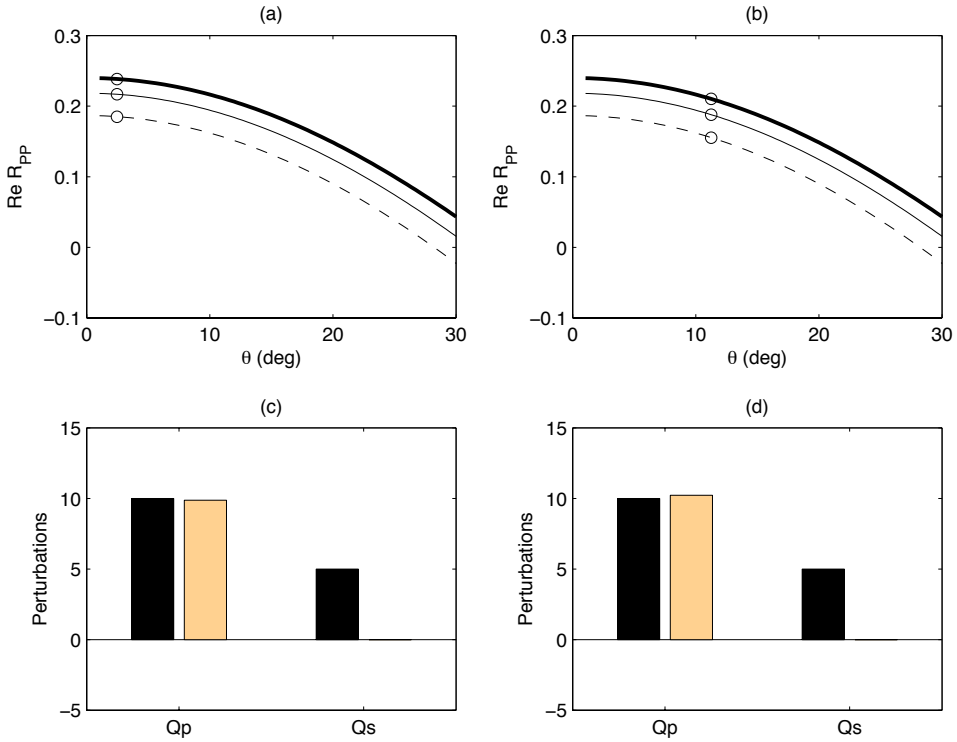

FIG. 20. R_{PP} anelastic inversion. (a)-(b) Three frequencies picked at two fixed angles as input. (c)-(d) Recovered (yellow) vs. exact (black) perturbations for Q_P and Q_S.

$$\Upsilon'_{\rho Qs}(\phi_0,\omega) = (4B-2)F_S(\omega)\sin^2\phi_0, \quad \Upsilon'_{\rho Qp}(\phi_0) = 0, \quad \Upsilon_{pp}(\phi_0) = 0,$$

$$\Upsilon'_{pQs}(\phi_0,\omega) = 0, \quad \Upsilon'_{pQp}(\phi_0,\omega) = 0, \quad \Upsilon'_{QsQs}(\phi_0,\omega) = \left[\frac{1}{4} + \left(\frac{7}{4} - 4B\right)\sin^2\phi_0\right] F_S^2(\omega),$$

and

$$\Upsilon_{QpQp}(\phi_0,\omega) = 0, \quad \Upsilon_{QpQp}(\phi_0,\omega) = 0.$$

Of particular note is the wealth of zero coefficients in the approximation. Target V_P and Q_P simply do not contribute to the amplitude prior to third order, in agreement with our previous experience with V_P alone in the the elastic case.

CONCLUSIONS

Amplitudes vary in seismic reflection data with tantalizing complexity. The full range of amplitude methods – from AVO analysis to full waveform inversion and inverse scattering – must be supported by theoretical descriptions that (1) provide the seismic explorationist with insight into the relationship between medium and amplitude, (2) lead directly to modeling and inversion algorithms, and (3) naturally allow the researcher to scale between rough-approximate (first order) and detailed-accurate (second order +) tools for analysis.

The benefit derivable from additional tools that fit this bill applies equally to AVO analysis in well-developed regimes, such as P-wave AVO, converted wave AVO and S-wave AVO, as to less fully developed model types, including anisotropic and anelastic regimes.

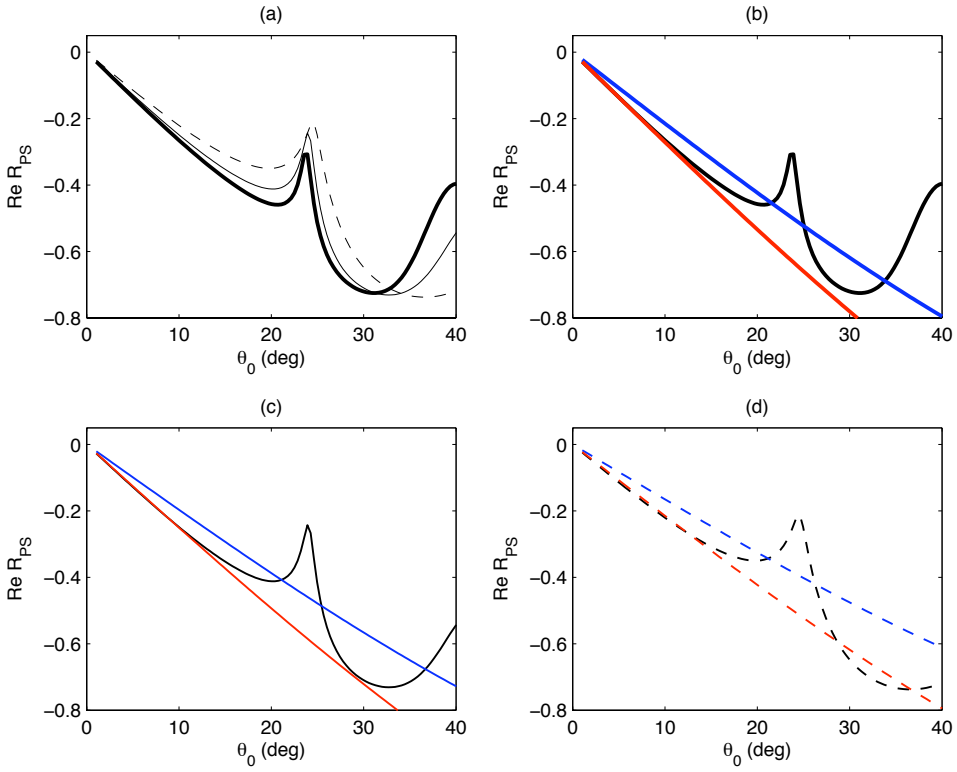

FIG. 21. Input R_{PS} curves for anelastic inversion: first order (blue), second order (red) vs. exact (black). (a) R_{PS} at three representative frequencies. (b)–(d) 1st, 2nd order, and exact coefficients at each frequency.

The purpose of this paper has been to extend and more completely formalize a mode of analysis of seismic amplitudes used to study anelastic inversion of P-P data, and to use it to make a series of points of analysis regarding (1) elastic P-wave, S-wave, and converted wave AVO behaviour, and (2) the influence of anelasticity both on these three aspects of AVO, and on their (now non negligible) AVF behaviour as well.

Specific predictions and/or results of analysis are as follows. First, mode conversions from contrasts in target Q_S alone will be non-negligible for relatively large contrast targets; contrasts in Q_P alone of a similar magnitude will cause negligible mode conversions. However, given a simultaneous contrast in both Q_P and Q_S, the target Q_P *will* influence the strength of the conversion non-negligibly.

We identify at second order the evident importance of a V_S/V_P value of 1/2, which is already well-known to be its rough expected value in many environments. We see that the coefficients of coupling between density and other parameters appear to involve the term $V_S/V_P - (1/2)$, which directly measures the deviation of this ratio from 1/2, and is nil when the true incidence medium V_S/V_P ratio is exactly 1/2.

The broadest technical point we wish to make is that *tools are available*, with which to model, invert, and comprehend seismic amplitudes in large contrast, nonlinear environments; tools which have not given up the practical interpretability of the linear Aki-Richards approximation.

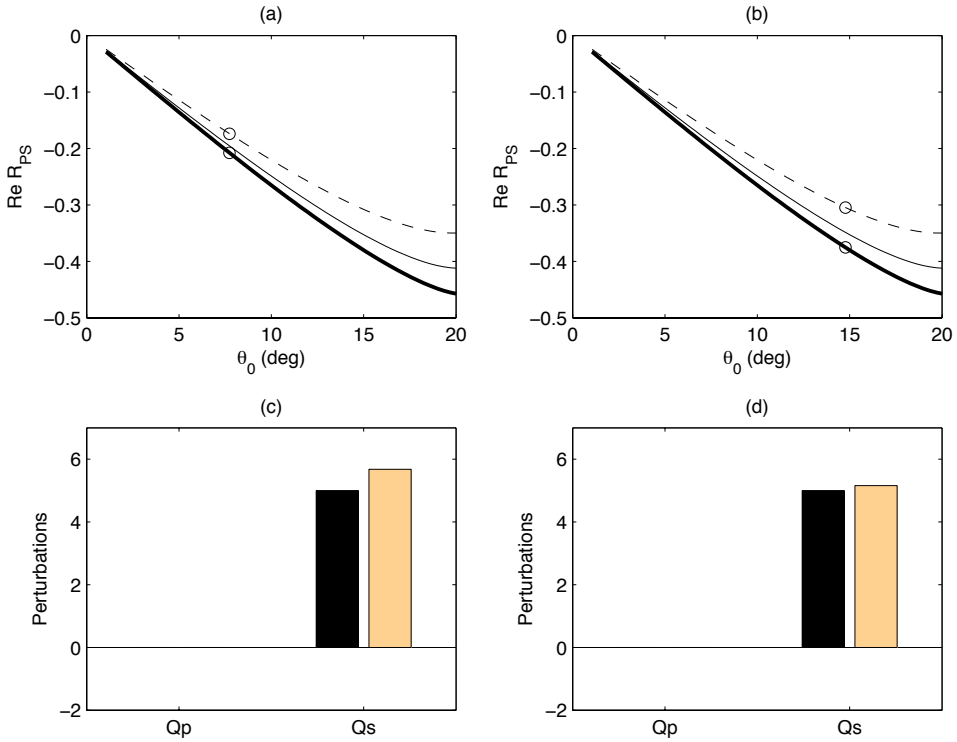

FIG. 22. R_{PS} anelastic inversion. (a)-(b) Two frequencies picked at two fixed angles as input. (c)-(d) Recovered (yellow) vs. exact (black) perturbations for Q_P and Q_S.

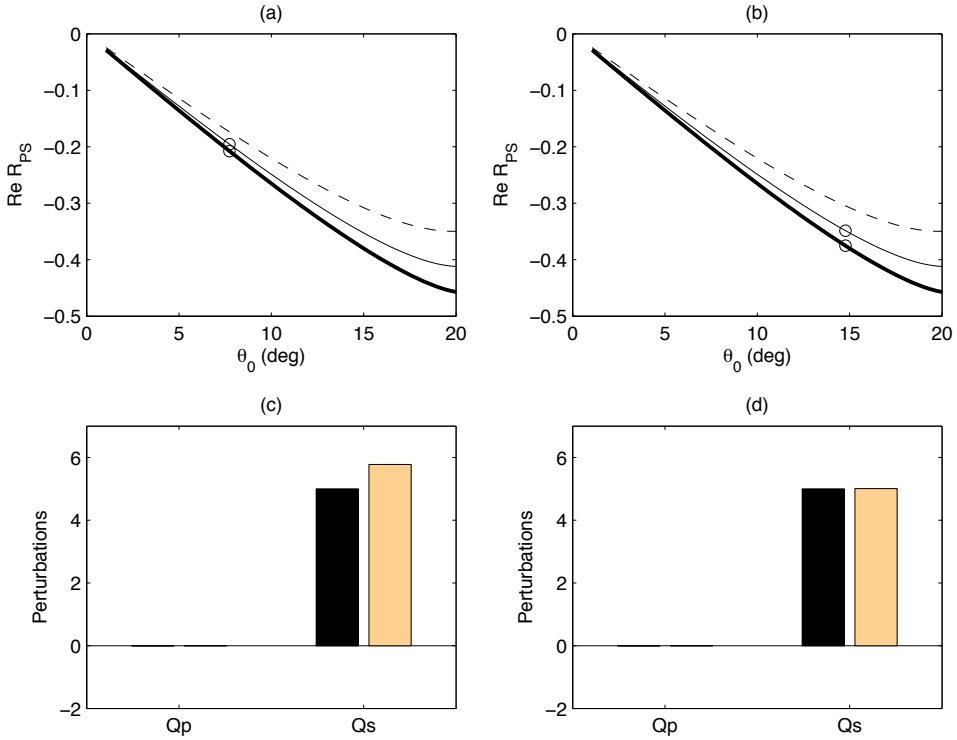

FIG. 23. R_{PS} anelastic inversion. (a)-(b) Two alternate frequencies picked at two fixed angles as input. (c)-(d) Recovered (yellow) vs. exact (black) perturbations for Q_P and Q_S.

Two primary streams of ongoing research are relevant here. First, these developments, which assume measurement of reflection coefficients as a function of angle being available, must be incorporated into a larger processing environment capable of handling panels of data: mapping large numbers of NMO corrected events from offset to angle, and either extracting as a function of time numerous curves interpretable as $R(\theta)$, or mapping our results and methods discussed here to a more general $R(x_h, t)$ domain. Second, we must continue with the systematic investigation of seismic data with well control to establish if and under what circumstances anelastic AVO/AVF behaviour is to be expected above the noise level. First steps in that direction have been discussed elsewhere in this report.

ACKNOWLEDGMENTS

The sponsors of CREWES and NSERC are gratefully acknowledged for their support of this research.

REFERENCES

Aki, K., and Richards, P. G., 2002, Quantitative Seismology: University Science Books, 2nd edn.

Bird, C., and Innanen, K. A., 2011, Field evidence for anelastic and dispersive AVF reflections: CREWES Annual Report (this report), **23**.

Borcherdt, R. D., 2009, Viscoelastic waves in layered media: Cambridge University Press.

Castagna, J. P., and Backus, M., 1993, Offset-dependent reflectivity: theory and practice of AVO analysis: SEG.

Chapman, M., Liu, E., and Li, X. Y., 2006, The influence of fluid-sensitive dispersion and attenuation on AVO analysis: Geophysical Journal International, **167**, No. 1, 89–105.

Haase, A. B., and Ursenbach, C. P., 2006, Spherical-wave AVO modeling in elastic and anelastic media: CREWES Annual Report, **18**.

Innanen, K. A., 2011a, Inversion of the seismic AVF/AVA signatures of highly attenuative targets: Geophysics, **76**, No. 1, R1–R11.

Innanen, K. A., 2011b, Matrix forms for the Knott-Zoeppritz equations: CREWES Annual Report (this report), **23**.

Lines, L. R., Sondergeld, C., Innanen, K. A., Wong, J., Treitel, S., and Ulrych, T. J., 2011a, Experimental confirmation of reflections on Q: CREWES Annual Report (this report), **23**.

Lines, L. R., Sondergeld, C., Innanen, K. A., Wong, J., Treitel, S., and Ulrych, T. J., 2011b, Experimental confirmation of "Reflections on Q": CREWES Annual report (this report), **23**.

Lines, L. R., Vasheghani, F., and Treitel, S., 2008, Reflections on Q: CSEG Recorder, **Dec**, 36–38.

Odebeatu, E., Zhang, J., Chapman, M., Liu, E., and Li, X. Y., 2006, Application of spectral decomposition to detection of dispersion anomalies associated with gas saturation: The Leading Edge, **2**, 206–210.

Quintal, B., Schmalholz, S. M., and Podladchikov, Y. Y., 2009, Low-frequency reflections from a thin layer with high attenuation caused by interlayer flow: Geophysics, **74**, N15–N23.

Ren, H., Goloshubin, G., and Hilterman, F. J., 2009, Poroelastic analysis of amplitude-versus-frequency variations: Geophysics, **74**, No. 6, N49–N54.

Stewart, R. R., Gaiser, J. E., Brown, R. J., and Lawton, D. C., 2002, Tutorial: converted-wave seismic exploration: methods: Geophysics, **67**, No. 5, 1348–1363.

Stewart, R. R., Gaiser, J. E., Brown, R. J., and Lawton, D. C., 2003, Tutorial: converted-wave seismic exploration: applications: Geophysics, **68**, No. 1, 40–57.

Waters, K. H., 1978, Reflection seismology: John Wiley & Sons, Inc.

Weglein, A. B., Araújo, F. V., Carvalho, P. M., Stolt, R. H., Matson, K. H., Coates, R. T., Corrigan, D., Foster, D. J., Shaw, S. A., and Zhang, H., 2003, Inverse scattering series and seismic exploration: Inverse Problems, **19**, R27–R83.

White, J. E., 1965, Reflections from lossy media: Journal of the Acoustical Society of America, **38**, 604–607.

Zhang, H., and Weglein, A. B., 2009, Direct nonlinear inversion of multiparameter 1D elastic media using the inverse scattering series: Geophysics, **74**, No. 6, WCD15–WCD27.